

1
2007

This is to certify that the
thesis entitled


EVALUATION OF APPLICATORS IN ROBOTICS SYSTEM
FOR CHEST WALL RECURRENCE BY FDTD SIMULATION

presented by

RUIHUA DING

has been accepted towards fulfillment
of the requirements for the

M.S. degree in ELECTRICAL ENGINEERING


Major Professor's Signature

Aug. 1, 2006

Date

MSU is an Affirmative Action/Equal Opportunity Institution

LIBRARY
Michigan State
University

PLACE IN RETURN BOX to remove this checkout from your record.
TO AVOID FINES return on or before date due.
MAY BE RECALLED with earlier due date if requested.

DATE DUE	DATE DUE	DATE DUE

**EVALUATION OF APPLICATORS IN ROBOTICS SYSTEM FOR CHEST WALL
RECURRENCE BY FDTD SIMULATION**

By

Ruihua Ding

A THESIS

**Submitted to
Michigan State University
in partial fulfillment of the requirements
for the degree of**

MASTER OF SCIENCE

Department of Electrical and Computer Engineering

2006

ABSTRACT

EVALUATION OF APPLICATORS IN ROBOTIC SYSTEM FOR CHEST WALL RECURRENCE BY FDTD SIMULATION

By

Ruihua Ding

Two kinds of applicators for hyperthermia on chest wall recurrence are evaluate by simulation in this thesis. One applicator is waveguide including 10m by 10cm and 10cm by 15cm operating at 915MHz, and the other is a 433MHz spiral antenna with a radius of 4.572cm. The simulations perform E-field calculations with the finite difference time domain (FDTD) method. In these 3D FDTD simulations, the patient models are derived from CT images, where material properties are assigned to tumor, skin, fat, and muscle tissues. The thickness and temperature of the water bolus and the position of the applicator are adjusted in these simulations, and a parametric study is performed on the resulting 3D patient model. Results show that the 433MHz spiral antenna generates larger thermal dose when the tumor is near the skin surface. For each applicator, the simulation results suggest the corresponding optimal configuration for different tumor target locations on the chest wall. Future efforts will incorporate these results into a comprehensive treatment planning system that optimizes the robot arm trajectory and combines these results with 3D visualization of static and dynamic temperature distributions on the chest wall.

© 2006

Ruihua Ding

All Rights Reserved

Dedicate the work to my parents.

ACKNOWLEDGMENTS

I would like to thank my thesis supervisor, Dr. Robert McGough, for giving me the chance to explore a research career in the field of biomedical applications. His continual support, technical insight, and dedication to this research has made this opportunity most enjoyable.

I would also like to thank Prof Leo Kemple, Edward Rothwell and Shanker Balasubramanian at the Michigan State University for being so accessible and helpful, for the guidance they provided during this research project, and for taking the time to explain the practical and clinical aspects of electromagnetics theory.

For providing all the clinical results and the data for simulation modelling, i thank the radiology department at Duke university, and also my lab fellows for being very helpful and supportive.

All the colleagues from the Biomedical Ultrasound and Electromagnetic Lab (BUEL) give me great support for the research and thesis writing.

TABLE OF CONTENTS

LIST OF TABLES	viii
LIST OF FIGURES	ix
1 Introduction	1
1.1 Hyperthermia for Breast Cancer	1
1.2 Existing HT Applicators	2
1.3 Robotic System	3
2 FDTD Modeling Techniques	5
2.1 Maxwell's Equations and the Yee Cell	5
2.2 Boundary Condition: Perfectly Matched Layer (PML)	8
2.3 PML for High Contrast Electromagnetic Material Model	11
2.4 Locally Conformal Models of Curved Surfaces	12
2.5 Simulation Models	13
2.5.1 Phantom Model from CT Images	13
2.5.2 Model from the Patient	15
3 The Optimization of System Parameters	21
3.1 BioHeat Transfer Equation (BHTE)	21
3.2 Thermal Dose	23
3.3 Optimization Object and Criteria	23
4 Applicator Heating Characteristics for Different Tumor Pattern and Location	26
4.1 System Description and Model	26
4.1.1 Superficial Hyperthermia Applicators	26
4.1.2 Water Bolus and Air Gap	29
4.2 Simulation Result of Phantom Model with Different Thickness of Tumor Layer	30
4.2.1 Waveguide Heating Effect	31
4.2.2 Spiral Antenna Heating Effect	35
4.3 Simulation Result of Tumor on Different Location	39

5	System Parameters Optimization Results for Spiral Antenna and Waveguide	51
5.1	Heating Effect of Spiral Antenna and Opimization	52
5.2	Heating Effect of Waveguide and Opimization	55
5.2.1	Water Bolus Only	56
5.2.2	Air Gap Only	57
5.2.3	Water Bolus and Air Gap	59
6	Conclusion and Future Work	67
6.1	Conclusion	67
6.2	Future Work	69
	BIBLIOGRAPHY	70

LIST OF TABLES

2.1	Parameters of Material and Human Tissue in FDTD Model.	16
3.1	Parameters of Material and Human Tissue in FDTD Model.	23
5.1	Parameters Study for Power Scale when Water Temperature is 40°C	53
5.2	Parameters Study for Power Scale when Water Temperature is 41°C	53
5.3	Parameters Study for Power Scale when Water Temperature is 42°C	53
5.4	Parameters Study for Water Bolus Thickness when Water Temperature is 42°C	56
5.5	Parameters Study for Air Gap Thickness when Air Temperature is 37°C	57
5.6	Parameters Study for Water Bolus Thickness when Water Temperature is 40.5°C	60

LIST OF FIGURES

1.1	Demonstration of the robotic arm movement and the modeling coordinates for human body	3
2.1	Cross section of the FDTD space lattice illustrating a PEC boundary diagonal with the cells.	13
2.2	One typical figure of CT images, based on which the phantom model is derived.	14
2.3	Two orthogonal CT images demonstrate the 3D model derived from CT scans. Left figure shows the xz plane, while right figure shows the yz plane. From the BOTTOM TO TOP, the different layers are water, skin, tumor, fat (in grey), and muscle (in white). The tumor phantom is 3cm inserted under the skin.	17
2.4	One typical figure of CT images obtained from the patient with chest wall recurrence. The white circle in this figure illustrate the possible tumor location.	18
2.5	Demonstration of 3D Anatomical Model Derived from Patient CT Images For Simulation. The green mesh represents the external contour. The red mesh shows the tumor region. The blue spiral on the left figure illustrates the spiral antenna's location, while the rectangular on the right figure illustrates the waveguide's location.	19
2.6	CT images that define the 3D patient model. Left figure shows the xz plane, while right figure shows the yz plane. From the BOTTOM TO TOP, the different layers are water, skin, tumor, fat (in grey), and muscle (in white). The tumor is represented by a 1cm thick phantom inserted under the skin.	20
4.1	Illustration of the spiral antenna applicator.	27
4.2	One figure on the xz plane of the human model based on the CT image with tumor and water bolus phantom	30

4.3	The simulated temperature distribution on the xz plane and yz plane in the center of the applicator by FDTD. The correspondent tumor layer is 1cm. The applicator applied here is a 10cm by 10cm waveguide working on 915MHz	41
4.4	The simulated temperature distribution on the xz plane and yz plane in the center of the applicator by FDTD. The correspondent tumor layer is 2cm. The applicator applied here is a 10cm by 10cm waveguide working on 915MHz	42
4.5	The simulated temperature distribution on the xz plane and yz plane in the center of the applicator by FDTD. The correspondent tumor layer is 3cm. The applicator applied here is a 10cm by 10cm waveguide working on 915MHz	43
4.6	The simulated temperature distribution on the xz plane and yz plane in the center of the applicator. The tumor layer is 1cm. The applicator applied here is a 4.572cm radius spiral antenna working on 433MHz .	44
4.7	The simulated temperature distribution on the xz plane and yz plane in the center of the applicator. The tumor layer is 2cm. The applicator applied here is a 4.572cm radius spiral antenna working on 433MHz .	45
4.8	The simulated temperature distribution on the xz plane and yz plane in the center of the applicator. The tumor layer is 3cm. The applicator applied here is a 4.572cm radius spiral antenna working on 433MHz .	46
4.9	The simulated temperature distribution on the xz plane and yz plane in the center of 10cm by 10cm waveguide. The maximum temperature is 7°C. Model is derived from the REGION ONE in Fig.1.1 with 1cm tumor layer and 3cm water.	47
4.10	The simulated temperature distribution on the xz plane and yz plane in the center of 10cm by 10cm waveguide. The maximum temperature is 7°C. Model is derived from the REGION TWO in Fig.1.1 tissue with 1cm tumor layer and 3cm water.	48
4.11	The simulated temperature distribution on the xz plane and yz plane in the center of 10cm by 10cm waveguide. The maximum temperature is 7°C. Model is derived from the REGION THREE in Fig.1.1 tissue with 1cm tumor layer.	49

4.12	The simulated temperature distribution on the xz plane and yz plane in the center of waveguide. The maximum temperature is 7°C. Model is derived from the REGION FOUR in Fig.1.1 tissue with 1cm tumor layer and 3cm water.	50
5.1	The simulated temperature distribution on the xz plane and yz plane in the center of the applicator. The model is derived from patient CT images. The applicator applied here is a 4.572cm radius spiral antenna working on 433MHz	63
5.2	The simulated temperature distribution on the xz plane and yz plane in the center of the applicator. The model is derived from patient CT images. The applicator applied here is a 10cm by 15cm of waveguide operating on 915MHz. Only water bolus exists in the system	64
5.3	The simulated temperature distribution on the xz plane and yz plane in the center of the applicator. The model is derived from patient CT images. The applicator applied here is a 10cm by 15cm of waveguide operating on 915MHz. Only air gap exists in the system.	65
5.4	The simulated temperature distribution on the xz plane and yz plane in the center of the applicator. The model is derived from patient CT images. The applicator applied here is a 10cm by 15cm of waveguide operating on 915MHz. Only air gap exists in the system.	66

CHAPTER 1

Introduction

1.1 Hyperthermia for Breast Cancer

Among all the cancer-related deaths of women, breast cancer ranks as the second cause, with lung cancer as the first one. According to American Cancer Society report in 2005, 211,240 new cases of invasive breast cancer are estimated to be diagnosed among women and breast cancer would lead to the death of 40,410 women[1]. Despite the treatment, cancer cells may grow again and this phenomenon is referred to as recurrence. About 5% to 40% of breast cancer patients would have chest wall recurrence (CWR) after mastectomy, which is followed by distant metastasis and death. The current survival rate from chest wall recurrence is only about 25% to 30%. Research shows that patients with CWR after 24 months have an optimistic prognosis, especially when they are treated by radiotherapy. Many patients with chest wall recurrence usually can not accept the full dose of radiotherapy because they have already been given the maximum radiation dose. Hyperthermia investigations have shown that cancer cells are more selectively sensitive to heat than normal cells. With the hyperthermia, there are more patients with tumors shrink completely with recurrent cancer than radiation treatment alone [2].

1.2 Existing HT Applicators

The existing applicators for superficial hyperthermia have advantages and disadvantages. The microwave waveguide applicator, usually a rectangular waveguide excited by a monopole feed, is a basic electromagnetic method for providing superficial hyperthermia. The dimensions of the waveguide are selected so that a strong TE₁₀ mode propagates at the chosen frequency. TE₁₀ mode is preferred because the electric field is oriented tangential to the different tissue interface, that can minimize the overheating of fat-muscle tissue interface due to the high resistance fat in parallel to the low resistance muscle or tumor layer [3] [4]. However, the field pattern of the standard waveguide is not uniform. Although later the horn waveguide was developed for a more uniform field pattern, they still suffered from being too large to effectively cover large regions of tissue over contoured treatment sites. The spiral antennas highly focus on the center of the spiral. To smooth out the centered energy to achieve useful heating over large area, a thick water bolus is required, which limits its use near complex contoured anatomy and increases setup complexity and the power required [5]. Inductive-loop current sheet applicator [6] which can be connected together in hinged flexible arrays for contoured surfaces, is more compact than waveguide and horn applicators but requires greater care when used in arrays to avoid under or overheating the area between the adjacent apertures. Contact Flexible Microstrip Applicator (CFMA) has the ability to conform the contoured treatment sites, but it is a single channel device without the ability to shape the specific absorption rate (SAR) pattern [8], [9] [7]. Conformal Microwave Array (CMA) is an array of Dual Concentric Conductor (DCC) microstrip patch antennas printed on very thin (9mm) and flexible printed circuit board(PCB) material. The feedline network needs lots of effort to build and control [10] [11] [12].

1.3 Robotic System

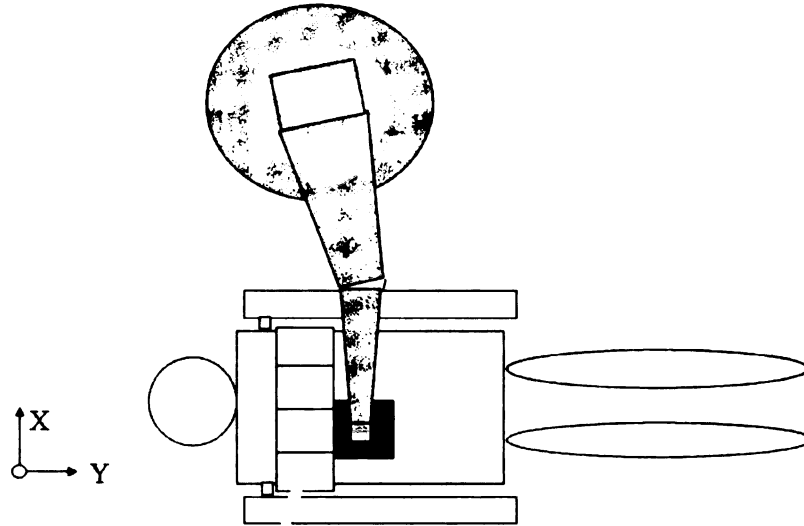


Figure 1.1. Demonstration of the robotic arm movement and the modeling coordinates for human body

All problems discussed in Sec.1.3 for existing HT applicators are caused by the non-uniform heating. The designs of applicator are getting more complexed for more uniform heating. For example, there are arrays of spiral antenna, complicated water bolus system. It can improve the heating effect but also increase the difficulty for fabrication and operation. In this paper, a robotically controlled prototype microwave system proposed achieve the uniform heating with the help of a robotic arm movement without increasing the complexity of electromagnetic applicator design. The prototype microwave robotic system for treating the chestwall recurrence is composed of a radio frequency(RF) applicator attached to a flexible robotic arm, shown as Fig. 1.1. The robot can repeat the desired scanning path throughout the thermal therapy session, automatically adjusting the treatment parameters in response to pa-

tient motion. The robotic movement enhances heat delivery across large areas and enables conformal thermal therapy for postmastectomy chestwall recurrence.

The following chapters focuses on studying the applicators which are going to be used in the robotic system later. One of them is 10cm by 15cm dimension rectangular waveguide working at 915MHz with the TE₁₀ mode. Another is 4.725cm radius spiral antenna operating at 433MHz with a 3mm substrate and a excitation probe inserted into the center of the substrate. Chap. 2 introduces how the models for simulation derived from CT images, which is the start point of FDTD simulation. It include all the key techniques for FDTD simulation for this specific biomedical problem. For the best thermal dose, two parameters of this hyperthermia system are studied. Chap. 3 introduces the optimization objects, goals and methods. Chap.4 describe the two applicators effect on tumors with varied thickness and location. The models in this chapter are derived from CT scans from Radiology Department of Michigan State University. There are also patients CT images obtained from Duke University Radio Oncology Department. Models derived from these patients are used for studying the optimization of system parameters. The optimization are described in Chap.5. And Chap.6 give conclusion for all the simulation results obtained in the thesis and give the outline for future work.

CHAPTER 2

FDTD Modeling Techniques

The method used for simulating the power deposition of the applicators is finite-difference time-domain(FDTD) method [13], which is widely used for the simulation of hyperthermia applicators[14]. With the known power deposition distribution, the temperature distribution can be obtained by the bio-heat transfer equation(BHTE) [15]. The thermal dose, which is based on the temperature distribution, is used to evaluate the effectiveness of hyperthermia applications.

The FDTD method is a numerical solution for Maxwell's curl equations, which are based upon volumetric sampling of the unknown electric and magnetic field within and surrounding the structure of interest over a period of time [13]. The key modeling techniques are introduced below.

2.1 Maxwell's Equations and the Yee Cell

The time-dependent Maxwell's equations are given in differential form by

$$\frac{\partial \bar{B}}{\partial t} = -\nabla \times \bar{E} - \bar{M} \quad (2.1)$$

$$\frac{\partial \bar{D}}{\partial t} = \nabla \times \bar{H} - \bar{J} \quad (2.2)$$

$$\nabla \cdot \bar{D} = 0 \quad (2.3)$$

$$\nabla \cdot \bar{B} = 0 \quad (2.4)$$

All the symbols in 2.1-2.4 are defined as:

- \bar{E} : electric field(volts/meter)
- \bar{D} : electric flux density(coulombs/meter²)
- \bar{H} : magnetic field(amperes/meter)
- \bar{B} : magnetic flux density (Weber/meter²)
- \bar{J} : electric current density(amperes/meter²)
- \bar{M} : equivalent magnetic current density (volts/meter²) discretization

In linear, isotropic materials, the relationship between \bar{D} , \bar{J} and \bar{E} , \bar{B} , \bar{M} and \bar{H} are:

$$\bar{D} = \epsilon \bar{E} = \epsilon_r \epsilon_0 \bar{E}; \quad \bar{B} = \mu \bar{H} = \mu_r \mu_0 \bar{H} \quad (2.5)$$

$$\bar{J} = \bar{J}_{\text{source}} + \sigma \bar{E}; \quad \bar{M} = \bar{M}_{\text{source}} + \sigma^* \bar{H} \quad (2.6)$$

where

- ϵ : electrical permittivity(farads/meter)
- ϵ_r : relative permittivity(dimensionless scalar)
- ϵ_0 : free-space permittivity(8.845×10^{-12} farads/meter)
- μ : magnetic permeability(henry/meter)
- μ_r : relative permeability(dimensionless scalar)
- μ_0 : free-space permeability($4\pi \times 10^{-7}$ henry/meter)
- σ : electric conductivity(semen's/meter)
- σ^* : equivalent magnetic loss(ohms/meter)

Substitute 2.5 and 2.6 into 2.1 and 2.2, Maxwell's curl equations becomes:

$$\frac{\partial \bar{H}}{\partial t} = -\frac{1}{\mu} \nabla \times \bar{E} - \frac{1}{\mu} (\bar{M}_{\text{source}} + \sigma^* \bar{H}) \quad (2.7)$$

$$\frac{\partial \bar{E}}{\partial t} = \frac{1}{\epsilon} \nabla \times \bar{H} - \frac{1}{\epsilon} (\bar{J}_{\text{source}} + \sigma \bar{E}) \quad (2.8)$$

In Cartesian coordinates, all the vector components in 2.7 and 2.8 can be decomposed into three scalar components.

$$\frac{\partial H_x}{\partial t} = \frac{1}{\mu} \left[\frac{\partial E_y}{\partial z} - \frac{\partial E_z}{\partial y} - (M_{\text{source}x} + \sigma^* H_x) \right] \quad (2.9a)$$

$$\frac{\partial H_y}{\partial t} = \frac{1}{\mu} \left[\frac{\partial E_z}{\partial x} - \frac{\partial E_x}{\partial z} - (M_{\text{source}y} + \sigma^* H_y) \right] \quad (2.9b)$$

$$\frac{\partial H_z}{\partial t} = \frac{1}{\mu} \left[\frac{\partial E_x}{\partial y} - \frac{\partial E_y}{\partial x} - (M_{\text{source}z} + \sigma^* H_z) \right] \quad (2.9c)$$

$$\frac{\partial E_x}{\partial t} = \frac{1}{\varepsilon} \left[\frac{\partial H_z}{\partial y} - \frac{\partial H_y}{\partial z} - (J_{\text{source}x} + \sigma E_x) \right] \quad (2.9d)$$

$$\frac{\partial E_y}{\partial t} = \frac{1}{\varepsilon} \left[\frac{\partial H_x}{\partial z} - \frac{\partial H_z}{\partial x} - (J_{\text{source}y} + \sigma E_y) \right] \quad (2.9e)$$

$$\frac{\partial E_z}{\partial t} = \frac{1}{\varepsilon} \left[\frac{\partial H_y}{\partial x} - \frac{\partial H_x}{\partial y} - (J_{\text{source}z} + \sigma E_z) \right] \quad (2.9f)$$

In 1966, Kane S. Yee developed central difference approximation for Maxwells curl equatons shown in Equ.2.9a to 2.9f. The finite-difference expressions for both space and time derivatives are simply programmed with second-order accuracy in the space and time increments. Function u of space and time is represented as

$$u(i\Delta x, j\Delta y, k\Delta z, n\Delta t) = u_{i,j,k}^n \quad (2.10)$$

where Δt is the time increment, assumed uniform over the observation interval, and n is an integer. Yee's expression for the first partial space derivative of u in x direction can be written as:

$$\frac{\partial u}{\partial x}(i\Delta x, j\Delta y, k\Delta z, n\Delta t) = (u_{i+1/2,j,k}^n - u_{i-1/2,j,k}^n)/(\Delta x) + O[(\Delta x)^2] \quad (2.11)$$

where $\pm 1/2$ denotes a space finite-difference over $\pm 1/2\Delta x$, meaning increment in the x direction. Yee's expression for the first partial time derivative of u at the fixed space point can be written as:

$$\frac{\partial u}{\partial t}(i\Delta x, j\Delta y, k\Delta z, n\Delta t) = (u_{i,j,k}^{n+1/2} - u_{i,j,k}^{n-1/2})/(\Delta t) + O[(\Delta t)^2] \quad (2.12)$$

where $\pm 1/2$ denotes a time finite-difference over $\pm 1/2\Delta t$, meaning increment in time. Based on the Yee cell theory, the central difference approximation for Maxwells curl

equations in the Cartesian coordinate can then be written in the form of finite difference equations.

2.2 Boundary Condition: Perfectly Matched Layer (PML)

In FDTD models for electromagnetic wave interaction problems in unbounded regions, an absorbing boundary condition (ABC) is introduced at the outer lattice boundary to simulate the extension of the lattice to infinity. In 1994, J.P. Berenger's has introduced a highly effective absorbing-material ABC called the perfectly matched layer(PML) [16]. Any plane waves of arbitrary incidence, polarization and frequency are matched at the boundary and can be ideally absorbed by this layer. To this end, Berenger derived a split-field formulation of Maxwell's equations where each vector field component is split into two orthogonal components. Each of the 12 resulting components is expressed as satisfying a coupled set of first-order partial differential equations. By choosing loss parameters consistent with a dispersionless medium, a perfectly matched planar interface is derived. In cartesian coordinates, the six field vector components E_x, E_y, E_z, H_x, H_y and H_z yield 12 subcomponents denoted as $E_{xy}, E_{xz}, E_{yx}, E_{yz}, E_{zx}, E_{zy}, H_{xy}, H_{xz}, H_{yx}, H_{yz}, H_{zx}, H_{zy}$. The three-dimensional(3D) time-domain Maxwell's equations for Berenger's split-field PML are:

$$\varepsilon \frac{\partial E_{xy}}{\partial t} + \sigma_y E_{xy} = \frac{\partial(H_{zx} + H_{zy})}{\partial y} \quad (2.13a)$$

$$\varepsilon \frac{\partial E_{xz}}{\partial t} + \sigma_z E_{xz} = -\frac{\partial(H_{yz} + H_{yx})}{\partial z} \quad (2.13b)$$

$$\varepsilon \frac{\partial E_{yz}}{\partial t} + \sigma_z E_{yz} = \frac{\partial(H_{xy} + H_{xz})}{\partial z} \quad (2.13c)$$

$$\varepsilon \frac{\partial E_{yx}}{\partial t} + \sigma_x E_{yx} = -\frac{\partial(H_{zx} + H_{zy})}{\partial x} \quad (2.13d)$$

$$\varepsilon \frac{\partial E_{zx}}{\partial t} + \sigma_x E_{zx} = \frac{\partial(H_{yz} + H_{yx})}{\partial x} \quad (2.13e)$$

$$\varepsilon \frac{\partial E_{zy}}{\partial t} + \sigma_y E_{zy} = -\frac{\partial(H_{xy} + H_{xz})}{\partial y} \quad (2.13f)$$

$$\mu \frac{\partial H_{xy}}{\partial t} + \sigma_y^* H_{xy} = -\frac{\partial(E_{zx} + E_{zy})}{\partial y} \quad (2.13g)$$

$$\mu \frac{\partial H_{xz}}{\partial t} + \sigma_z^* H_{xz} = \frac{\partial(E_{yz} + E_{yx})}{\partial z} \quad (2.13h)$$

$$\mu \frac{\partial H_{yz}}{\partial t} + \sigma_z^* H_{yz} = -\frac{\partial(E_{xy} + E_{xz})}{\partial z} \quad (2.13i)$$

$$\mu \frac{\partial H_{yx}}{\partial t} + \sigma_x^* H_{yx} = \frac{\partial(E_{zx} + E_{zy})}{\partial x} \quad (2.13j)$$

$$\mu \frac{\partial H_{zx}}{\partial t} + \sigma_x^* H_{zx} = -\frac{\partial(E_{yz} + E_{yx})}{\partial x} \quad (2.13k)$$

$$\mu \frac{\partial H_{zy}}{\partial t} + \sigma_y^* H_{zy} = \frac{\partial(E_{xy} + E_{xz})}{\partial y} \quad (2.13l)$$

If x or y or z are replaced by w , then σ_w, σ_w^* become homogeneous with respect to the electric and magnetic conductivities. To satisfy the matching condition at a normal-to- w PML interface in the lattice, the σ_w, σ_w^* pair has to satisfy:

$$\sigma_x^* / \mu = \sigma_x / \varepsilon \quad (2.14)$$

$$\sigma_y^* / \mu = \sigma_y / \varepsilon \quad (2.15)$$

$$\sigma_z^* / \mu = \sigma_z / \varepsilon \quad (2.16)$$

In continuous space, the PML absorber and the host medium are perfectly matched. But in FDTD lattice, electric and magnetic material parameters are represented discretely, which will result in discretization errors. Berenger proposed spatial

scaling of the PML parameters to reduce the discretization errors at material interfaces. The conductivity in the PML cells increases from zero at the vacuum-layer interface to a value σ_m at the outer side of the layer. And for each layer, the conductivity can be calculated by:

$$\sigma(\rho) = \sigma_m \left(\frac{\rho}{\delta}\right)^n \quad (2.17)$$

where δ is the PML thickness, ρ is the depth of this layer in PML. The theoretical reflection coefficient of PML at normal incidence is

$$R_0 = \exp\left(-\frac{2}{\varepsilon_0 \varepsilon_r c} \int_0^\delta \sigma(\rho) d\rho\right) \quad (2.18)$$

where $\sigma(\rho)$ indicates the PML conductivity parameter at the point of ρ , c means the speed of wave propagation in the air. $\varepsilon_0 \varepsilon_r$ shows the conductivity in the host medium. Substitute 2.17 into 2.18, σ_m can be calculated as:

$$\sigma_m = -\frac{(n+1)\varepsilon_0 \varepsilon_r c \ln(R_0)}{2\delta} \quad (2.19)$$

R_0 is desired reflection error; n is the order of PML. Typically, $3 \leq n \leq 4$ has been found to be nearly optimal for many FDTD simulations. For a broad range of applications, an optimal choice for a 10-cell-thick, polynomial-graded PML is $R = e^{-16}$; for 5-cell-thick PML, $R_0 = e^{-8}$. For my simulation, 16-cell layer with R_0 equal to e^{-16} gives good results.

PML performs best when the conductivity profile is averaged over each grid cell. In this case, conductivity of $\sigma(\rho)$ can be analytically integrated over one grid cell, and divided by the cell thickness d . Take x direction for example, the conductivity for the i_{th} cell in PML can be calculated by:

$$\sigma_{x(i)} = \frac{1}{d} \int_{x(i)-d/2}^{x(i)+d/2} \sigma_x(\rho) d\rho \quad (2.20)$$

where the $\sigma_x(\rho)$ is obtained by 2.17

2.3 PML for High Contrast Electromagnetic Material Model

The PML described in sec.2.2 is ideal for uniform material, which means the material in front of the PML has uniform electromagnetic characteristic parameters. In this model, the human tissue like the skin, tumor and so on has different permittivities. The PML for the human body can be chosen as non-uniform PML. In the non-uniform PML, the permittivity and permeability are different from point to point. These parameters are defined from each point in front of the layer instead of each layer. Non-uniform PML will consume too much computer time and memory space, which is not practical for this problem. An approximation is used in the model. Because of the electromagnetic characteristic parameters of human tissue including the permittivity and permeability are very close to those of water, assume the human tissue is surrounded by water and then build the PML according to water's EM parameters. This assumption will bring reflection between the water and human tissue by the water which does not exist in the real problem. However, the reflection is small enough to approximate the real temperature distribution for the parameters of water and human tissue is close.

In the configurations, there is air between the applicator and human body. The EM parameters of air are sharp contrast with the ones of human tissue, which would leads to bigger reflection than water. One solution is modeling the the surrounding air layer far away from human tissue. The human tissue is lossy material, if the simulation domain is large enough that the field is very small at the interface of the human tissue and the assumed air. When the waveguide is 15cm by 10cm, the human body tissue is chosen as 18cm by 12cm, which is surrounded by air. To test the error bring by the assumed air, a test model is built here. In this model, a 18cm by 12cm human body is derived from the CT images. The waveguide is built 4cm above

the chest surface. The source of the waveguide is chosen as pulse source which lasts only 50 timesteps. The simulation can show the reflection by the proposed air if the reflection is obvious. The FDTD simulation can show the EM field from step to step, from which there is no reflection. The power depostion in human tissue after 3000 timesteps is -58.4dB compared with the highest power generated in the simulation, which means the reflection is very small enough for the simulation to approach the real temperature distribution.

2.4 Locally Conformal Models of Curved Surfaces

According to Sec. 2.1, the cubic Yee cell leads to the staircased mesh, which brings numerical error when the arbitrarily shaped surface is not aligned with major grid planes. The locally conformal modeling technique introduced by Dey and Mittra (DM) achieves more accuracy for an arbitrary surface than the Yee cell grid [13], [17]. The implementation of this new modeling method is described below, which is used for modeling the spiral antennas in this paper.

Fig. 2.1 demonstrates the general cell for Dey-Mittra technique, where the diagonal line shows the PEC surface intersect with the classic FDTD cells. Based on the integral form of Faraday's law, the updated equation for H is as follows:

$$H_z \big|_{-\Delta x/2, \Delta y/2}^{n+1/2} = H_z \big|_{-\Delta x/2, \Delta y/2}^{n-1/2} + \frac{\Delta t}{\mu_0 A} (E_x \big|_{-\Delta x/2, \Delta y}^n \cdot f - E_x \big|_{-\Delta x/2, 0}^n \cdot g - E_y \big|_{-\Delta x, \Delta y/2}^n \Delta y) \quad (2.21a)$$

where area A and distance f and g are defined as in Figure2.1

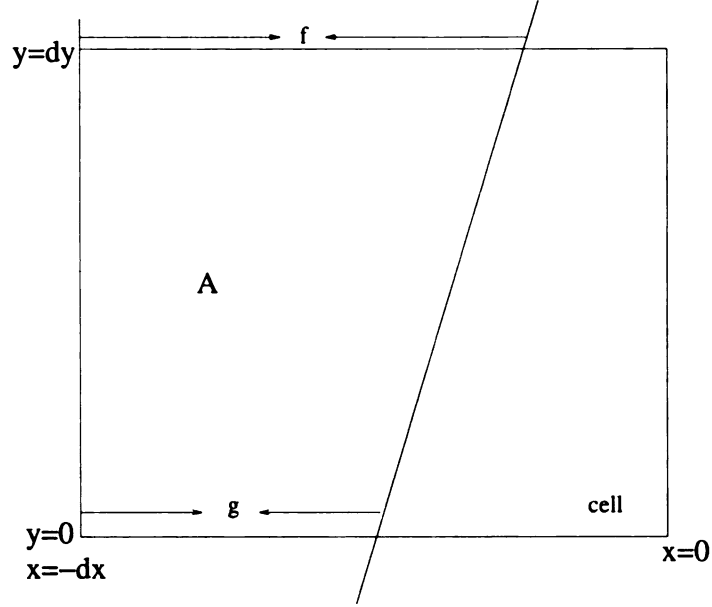


Figure 2.1. Cross section of the FDTD space lattice illustrating a PEC boundary diagonal with the cells.

2.5 Simulation Models

2.5.1 Phantom Model from CT Images

For the first stage of simulation, there are CT images from Radiology Department of Michigan State University. Human tissue model is derived from these CT scans. By inserting the tumor phantom into these model, the applicator's effect on human body can be studied. The phantom model built in this section is better than the flat tissue layers phantom for study the heating effect on human body. Based on this phantom model, the effect of the waveguide and spiral antenna on different tumor thickness pattern and different location is studied.

In the numerical simulation, human models are derived from the 47 slices of CT scan from Radiology Department of Michigan State University. One of these CT images shown in Fig.2.2 has a resolution of 512 by 512 pixels with 0.97mm spacing

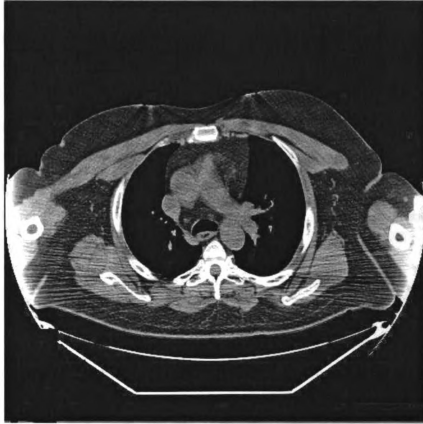


Figure 2.2. One typical figure of CT images, based on which the phantom model is derived.

between the adjacent pixels thus having 500mm by 500mm field of view (FOV). These 47 slices cover a region of 150mm along the long axis (y axis) of the body. This region is selected 10cm below the shoulder, where tumor is usually located. The human tissues such as the fat, muscle and bone are specified by the different gray scale intensities. Based on the real tumor pattern, phantom tumor with 1cm, 2cm and 3cm thickness is chosen to insert under the skin as a typical model, which means the tumor layer conforms having the skin with variable thickness along z direction.

For the simulation, radius of the spiral antenna is 5cm, and the waveguide is 10cm by 10cm on the transverse face. Due to the electromagnetic power penetration depth, 12cm along the x axis and 12cm along the y axis is enough for the numerical simu-

lation. Simulation and experimental results show that temperature rise in the region below 5cm under the skin is much less than 0.1 Celsius with the largest temperature rise is 7 degree. In model, human body is 5cm along the z direction. The total model size is 12cm by 12cm by 10cm along x, y and z axis respectively.

The heated region is no larger than 10 cm by 10cm, and a robotic arm movement is necessary for the uniform heat around the whole chest region. According to the size of the chest and the heated region, the chest is separated into four region, label in Fig.1.1. For simulation, all of the four layers are taken under consideration to test the heating effect of these two applicators.

2.5.2 Model from the Patient

Human tissue model derived from patients with chest wall recurrence will be better reference for treatment plan and accurate model. In the second stage of the simulation, CT images from a patient in Duke cancer center are available. Based on patient model, the optimization of the system parameters such as water bolus and air gap thickness, their temperature. Based on the simulation result, the water bolus and air gap can be combined for better thermal dose.

For better reference for treatment plan and accurate model, data obtained from a patient with chest wall recurrence is more useful. For this purpose 75 CT images were obtained from a patient in Duke cancer center. Fig. 2.4 shows one typical image. The white circle in the figure indicates recurrence of the tumor near the chest wall from where the breast has been removed. Different tissues are classified based on the varying image in tensity levels. The intensity of tumor closely resembles that of muscle therefore, then it is identified base on the doctor's suggestion. Since the tumor is randomly distributed, a phantom tumor layer is inserted at possible tumor location obtained from the image.

From the simulation result of phantom model, the heating effect is better when the

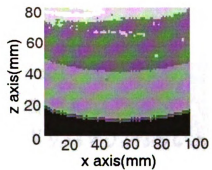
<i>Material/ Tissue</i>	<i>Permittivity ϵ_r</i>	<i>Conductivity $\sigma (S \cdot m^{-1})$</i>	<i>Density $\rho (kg \cdot m^{-3})$</i>
Skin	2.1	0.69	1010
Fat	11.6	0.08	920
Muscle	75	0.75	1041
Tumor	65	0.74	1177
Water	76.5	0.001	1000
Metal	1	10^{-7}	7900

Table 2.1. Parameters of Material and Human Tissue in FDTD Model.

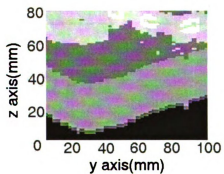
applicator is parallel to the human contour. For FDTD modeling, the RF applicators are modeled in a way such that they are parallel or perpendicular to the FDTD grid, which is easier for source modeling. Then the human body needs to be rotated to a position that parallel with the RF waveguide or spiral antenna. The 3D image of the final model is shown in Fig. 2.5. The green mesh represents the external contour, the red mesh shows the tumor region and the blue spiral on the left figure illustrates the location of spiral antenna, while the rectangle on the right figure illustrates the location of waveguide. The black line indicates the area defined for FDTD simulations.

Since the radius of the spiral antenna is 5cm, and the waveguide here is 10cm by 15cm on the transverse face, the numerical simulation domain is 12cm in the x direction and 17cm in y direction. In z axis the human model in model is 5cm due to the penetration depth. Water bolus or air gap is always used in treating the tumor in order to obtain evenly distributed heating pattern, therefore properties of water or air surrounding the human body are also included in the model. In order to have water bolus or air gap with variable thickness, the simulation domain in Z direction is 10cm. The whole simulation domain is extracted from the model shown in Fig. 2.5. Two orthogonal images from this region of interest are shown in Fig.2.6.

The electrical parameters for all the materials in FDTD simulation are listed in Table 2.1. [18]



(a) xz plane



(b) yz plane

Figure 2.3. Two orthogonal CT images demonstrate the 3D model derived from CT scans. Top figure shows the xz plane, while bottom shows the yz plane. From the BOTTOM TO TOP, the different layers are water, skin, tumor, fat (in grey), and muscle (in white). The tumor phantom is 3cm inserted under the skin.

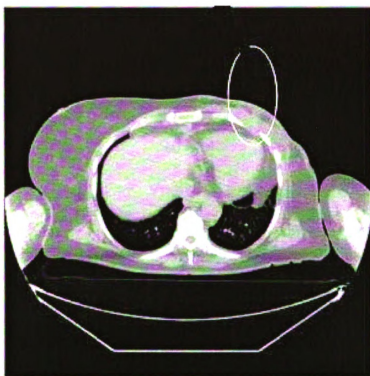
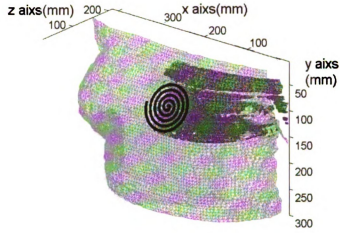
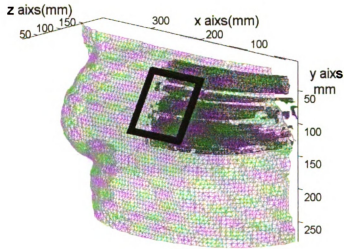


Figure 2.4. One typical figure of CT images obtained from the patient with chest wall recurrence. The white circle in this figure illustrate the possible tumor location.

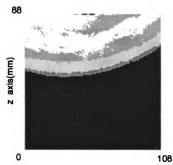


(a) spiral

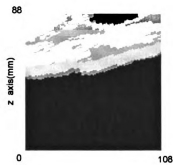


(b) waveguide

Figure 2.5. Demonstration of 3D Anatomical Model Derived from Patient CT Images For Simulation. The green mesh represents the external contour. The red mesh shows the tumor region. The blue spiral on the left figure illustrates the spiral antenna's location, while the rectangular on the right figure illustrates the waveguide's location.



(a) xz plane



(b) yz plane

Figure 2.6. CT images that define the 3D patient model. Left figure shows the xz plane, while right figure shows the yz plane. From the BOTTOM TO TOP, the different layers are water, skin, tumor, fat (in grey), and muscle (in white). The tumor is represented by a 1cm thick phantom inserted under the skin.

CHAPTER 3

The Optimization of System Parameters

3.1 BioHeat Transfer Equation (BHTE)

The standard thermal diffusion equation proposed by Pennes [15] described the effect of metabolism and blood perfusion on the energy balance within tissue.

$$\rho c \frac{\partial T}{\partial t} = \nabla \cdot \kappa \nabla T + c_b \omega_b (T_a - T) + Q_{EM} \quad (3.1)$$

where ρ is the mass density, with the unit of kg/m^3 . c is the specific heat. T is the temperature of the tissue. T_a is the temperature of the blood. κ is the thermal conductivity. c_b means the thermal conductivity of blood. ω_b is the blood perfusion, with the unit of $kg/m^3/s$. The BHTE is also written in another form as:

$$\rho c \frac{\partial T}{\partial t} = \nabla \cdot \kappa \nabla T + (\rho_b c_b) \rho \omega (T_a - T) + Q_{EM} \quad (3.2)$$

where ρ is the mass density, with the unit of kg/m^3 . ρ_b means the mass density of blood, with the unit of kg/m^3 . ω is the blood perfusion rate, with the unit of $m^3/kg/s$. Relation of blood perfusion and perfusion rate is given by:

$$\omega_b = \rho_b \rho \omega \quad (3.3)$$

With this relationship, Eqn 3.2 becomes similar to Eqn. 3.1.

In the BHTE above, Q_{EM} is the heat generation rate due to the deposited EM power, which can be calculated by:

$$Q_{EM} = \frac{\sigma}{2}|E^2| \quad (3.4)$$

where σ is the electrical conductivity of the biological tissue.

To obtain the transient temperature distribution, 3.2 is rewritten into the following form by the Finite-Difference method:

$$\begin{aligned} \rho c \frac{T^{n+1}(i, j, k) - T^n(i, j, k)}{\Delta t} = & \frac{k}{\Delta^2} [T^n(i+1, j, k) + T^n(i-1, j, k) \\ & + T^n(i, j+1, k) + T^n(i, j-1, k) + T^n(i, j, k+1) \\ & + T^n(i, j, k-1) - 6T^n(i, j, k)] \\ & + Q_{EM} - \rho_b C_b \omega T^n(i, j, k) \end{aligned} \quad (3.5a)$$

where Δt means the time step, Δ means the space step. Since the time step difference of the finite difference time domain method is $dx/2c$, which is too small for the temperature to reach the steady state. To accelerate the iteration process to obtain the steady state temperature distribution, multiply the Eqn.3.5b with a factor α and simplify as:

$$\begin{aligned} T^{n+1}(i, j, k) = & \frac{k}{\rho C} \frac{\alpha \Delta t}{\Delta^2} [T^n(i+1, j, k) + T^n(i-1, j, k) \\ & + T^n(i, j+1, k) + T^n(i, j-1, k) + T^n(i, j, k+1) + T^n(i, j, k-1)] \\ & + [1 - (6 \frac{k}{\rho C} \frac{\alpha \Delta t}{\Delta^2} + \frac{\alpha \Delta t}{C} \rho_b C_b \omega)] T^n(i, j, k) + \frac{\alpha \Delta t}{\rho C} Q_{EM} \end{aligned} \quad (3.6a)$$

According to the definition above, all the heat parameters used in these simulations are listed in Table 3.1[18]. The thermal conductivity of blood c_b is 3840 W/K/m and the mass density of blood ρ_b is 1060 kg/m^3 .

The factor α is chosen to satisfy

$$\alpha \Delta t < \frac{(\Delta x)^2 \rho c}{6\kappa} \quad (3.7)$$

<i>Material/ Tissue</i>	<i>Thermal Conductivity κ ($W \cdot K^{-1} \cdot m^{-1}$)</i>	<i>Specific Heat c ($J \cdot K^{-1} \cdot kg^{-1}$)</i>	<i>Blood Perfusion Rate ω ($kg^{-1} \cdot m^3 \cdot s^{-1}$)</i>
Water	0.55	4810	0
Skin	0.266	3430	$2.0 \cdot 10^{-6}$
Fat	0.223	2325	$0.467 \cdot 10^{-6}$
Muscle	0.4975	3720	$0.63 \cdot 10^{-6}$

Table 3.1. Parameters of Material and Human Tissue in FDTD Model.

The differential equation can be used to calculate the time variant temperature distribution. Simulation results show that temperature reaches to steady state after 10 minutes, and the treatment lasts 60 minutes. Therefore the time varying temperature distribution is necessary to obtain an accurate thermal dose.

3.2 Thermal Dose

The parameter used for evaluating the effectiveness of these two applicators is thermal dose, which is defined by

$$D(T, t) = \int_0^{tf} R^{(43-T(t))} dt \quad (3.8)$$

where T stands for temperature and t stands for time. R is 0.25 when the temperature is smaller than 43 degree Celcius and 0.5 when it is larger, and tf is the heating period. The unit of thermal dose is the equivalent number of minutes at 43 degree Celcius. From Eqn. 3.8, the thermal dose characterizes the combined effect of the temperature and treatment time, which is widely used for evaluating the heating effect of hyperthermia for cancer therapy treatment.

3.3 Optimization Object and Criteria

To control the temperature on the surface area of the skin during treatment, water bolus or air flow or both are used between the applicator and the patient. The

thickness of water bolus and air gap effects the power deposition distribution in the human body due to the impedance match effect. When the thickness of water gap or air gap is different, the reflection on the interface is different, which effects the field distribution in the tumor layer. The interface of human body and the water or air is not flat, and the human tissue is inhomogeneous media. Then the analytical solution of the ideal thickness of water bolus or air gap can not be obtained. Only by the simulation the optimized thickness can be obtained for the best thermal dose. This is the first object of the optimization.

The water temperature and air gap temperature also affects the temperature distribution in the human body because of the blood perfusion. If the temperature is too high, it will burn the skin. If the temperature is too low, it can cool the skin but will lower the temperature distribution. Meanwhile, the temperature of water bolus also effect the highest the temperature in the human body. To adjust the highest temperature lower than 45°C , the power scale needs to be adjusted. In other words, if the water temperature is high, the power scale will lower down; if the water temperature is low, the power scale should rise. Which combination of the water temperature and power scale give the best thermal dose, this is another object of the optimization.

The first and second object is irrelevant with each other from the simulation results. In the simulation, after obtaining one power deposition distribution of one model, a series of water temperature is modeled for different water bolus thickness. The result shows the thermal dose pattern of different water bolus thickness are same when the water temperature varies.

Therefore for the first objective, ignore the heat diffusion of surrounding material such as water and air and choose the one that gives the best thermal dose. When the surrounding material is same as human body temperature, it is easier to implement in BHTE model and also show the heating pattern of the applicator only. The water bolus thickness varies from 0.5cm to 3cm, and the air gap thickness varies from 0.5cm

to 2cm according to clinical results. The second object is implemented after choosing the optimized water bolus thickness. Adjust the temperature of water or air flow surrounding the patient varying from 37 to 43°C. The goal is to obtain the best the thermal dose and give the patients safe and comfort heating pattern. The criteria are the following. Maximize the TD90 (mineq43°C), which means the thermal dose for 90% tumor coverage based on 60 minutes accumulated treatment time. For the same treating segment, the thermal dose of 10% of normal tissue is called TD10, which should be 5 times smaller than the TD90 minutes. The temperature above 45°C is toxic for human body, so that no human tissue is exposed to above 45 °C. The highest temperature in skin tissue must below 43°C considering the patient's comfort.

CHAPTER 4

Applicator Heating Characteristics for Different Tumor Pattern and Location

4.1 System Description and Model

The robotic system is introduced in this section, including the Radio-Frequency(RF) applicators, the water bolus and air gap located between human body and the applicators.

4.1.1 Superficial Hyperthermia Applicators

Waveguide and Archimedean spiral antennas are chosen as the applicators used in the robotic system.

Two waveguides of different sizes are studied in this thesis, which are 10cm by 10cm and 10cm by 15cm. All waveguides work in TE₁₀ mode at 915MHz. The electric field(E field) distribution for the waveguide is:

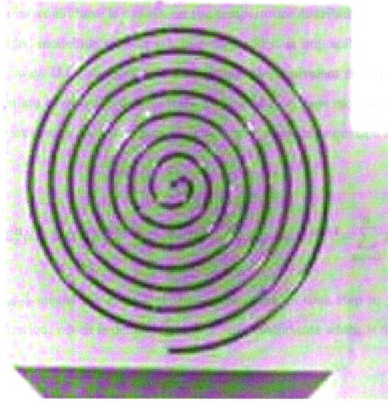


Figure 4.1. Illustration of the spiral antenna applicator.

$$E = E_0 \sin(\omega) \quad (4.1)$$

E_0 satisfy when it is TE10 mode:

$$E_0 = E_a \sin\left(\frac{\pi x}{a}\right) \quad (4.2)$$

where x stands for the field point distance and a stands for the length in x direction.

There are two ways of modeling the excitation of applicators, i.e. hard source and soft source modeling. For waveguide, the hard source modeling is realized by setting the node to a specific value shown in 4.2. The equivalent source wall itself is equivalent to PEC, which would bring wave reflection if the wave is incident on this source plane. For water surrounded modeling, the wavelength is small enough

to build the source wall far away from human tissue layer, then the reflection caused by the hard source would have low effect on the temperature distribution calculation. For air surrounded modeling, wavelength increases and it is impossible to build the source plane far way. If for the soft source modeling, the equivalent electric source is difficult to calculate to give the field exactly as Eqn. 4.2. A new modeling technique called transparent source modeling is used. The source modeling equation for FDTD is:

$$E_z^{n+1}(i_{\text{src}}) = E_z^n(i_{\text{src}}) + Zs[H_y^{n+1/2}(i_{\text{src}}) + H_y^{n+1/2}(i_{\text{src}}-1)] + f^{n+1} - \sum_{m=0}^n I^{n-m+1} f^m. \quad (4.3)$$

where $E_z^n(i_{\text{src}})$ means the E field at the source point on time step n; f^n stands for the source function, which is defined by 4.2. I^n are coefficients which is defined by:

$$I^0 = 0 \quad (4.4)$$

$$I^1 = 1 - 2s^2 \quad (4.5)$$

$$I^2 = -2s^2 + 2s^4 \quad (4.6)$$

$$I^3 = -2s^2 + 6s^4 - 4s^6 \quad (4.7)$$

$$I^4 = -2s^2 + 12s^4 - 20s^6 + 10s^8 \quad (4.8)$$

$$I^5 = -2s^2 + 20s^4 - 60s^6 + 70s^8 - 28s^{10} \quad (4.9)$$

Here $s = \frac{1}{2}$, and I^5 is as small as 0.0586, and $I^6, I^7...$ can be ignored in my simulation.

The Archimedes' spiral antenna is shown as Fig.4.1. The polar equation used to describe the Archimedes' spiral is:

$$r = a\theta \quad (4.10)$$

For this applicator, the radius a is 0.143cm and the strip width of the antenna is 0.53cm. θ goes from 0 to 10π . The diameter is approximately 9.144cm. The substrate thickness is 3mm. And the feed point of the antenna is in the center of the antenna.

Soft source modeling is used for modeling the spiral antenna. The equivalent electrical source for modeling is defined by:

$$E = U/d \quad (4.11)$$

The equivalent source is located at the probe which is attached to the center of the spiral antenna.

4.1.2 Water Bolus and Air Gap

To control the temperatures on the skin, water bolus or airflow is needed between the applicator and human body. For modeling the water bolus, an assumption is made that the water in the bolus can maintain a constant temperature by a water control system. For electromagnetic simulation, the water bolus is modeled as water surrounding the human tissue, which works as an impedance match. The thickness of the bolus varies from 0cm to 3cm. For BHTE simulation, the heat fluxes between the skin and the water, which leads to the heating or cooling effect on patient. To achieve a better thermal dose, water temperature is preferred above $37^{\circ}C$. Human skin can not bare temperature above $43^{\circ}C$. Therefore water temperature is between $37^{\circ}C$ to $43^{\circ}C$.

In clinical center, the air flow is used between the applicator and human body without water bolus. For similar reason of water bolus, the air gap distance varies from 0.5cm to 3cm and the temperature of evaporation also varies from $37^{\circ}C$ to $43^{\circ}C$.

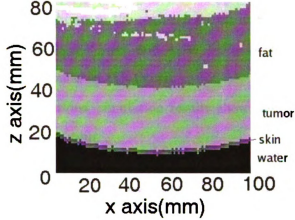


Figure 4.2. One figure on the xz plane of the human model based on the CT image with tumor and water bolus phantom

4.2 Simulation Result of Phantom Model with Different Thickness of Tumor Layer

In this section, human model is derived from a male CT data. The purpose is to develop the simulation system, including model from CT images, FDTD simulation for two different applicators, FD-BHTE for thermal dose and the optimization of water bolus thickness. To study the applicator's penetration depth, three different thicknesses, 1cm, 2cm and 3cm tumor layer are inserted into the human model as a phantom. The water bolus thickness effect the EM power deposition and therefore the thermal dose distribution. Then in these models the water bolus thickness varies to obtain the thickness which gives the best thermal dose. For each thickness of tumor phantom, the water bolus thickness varies from 3cm to 6cm.

Fig.4.2 illustrats one of these models composition with two orthogonal planes from the center position. The model size is 12cm by 12cm by 12cm, while the tumor is 3cm and water bolus is 4cm. Fig.4.2 shows the xz plane at the center of the model.

Along the z axis, from 0 to 8 cm, water, skin, tumor, fat and muscle layers are present which are represented with different intensities in the figure. This model is based on the human body contour shown in the region 1 shown in Fig.1.1. For other models, just the thickness of the tumor layer and water bolus is changed, while the layer distribution sequence is similar to this figure.

In the next two subsections, simulation results show the optimized water bolus thickness for each tumor phatom.

4.2.1 Waveguide Heating Effect

A 10cm by 10cm waveguide excited with a TE₁₀ mode is applied to the human model. In this section, the simulation results show the optimized water bolus thickness for each tumor layer thickness and the corresponding temperature distribution.

Based on the model derived in Chap. 2.5.1, a 1cm thickness tumor layer phantom is inserted under the skin layer of the human tissue model extracted from CT scans. Set the water bolus from 3cm to 6cm. Obtain different electromagnetic power depositions for these four different water bolus thicknesses. The best water bolus thickness 3cm gives the best TD₉₀, i.e.thermal dose for 90 percent of the tumor tissue, with a specific treatment time. To illustrate the heating pattern of the waveguide for 1cm tumor, the temperature distribution on 2 orthogonal planes is shown in the Fig. 4.3 for 1cm thickness of tumor layer and 3cm thickness of water bolus. The coordinates is shown in 2.5, from which XZ plane shows the top view of the chest while YZ plane shows the side view of the chest. The top figure shows the temperature distribution on XZ plane which locates at the center of the waveguide. Along Z axis, the region length is 8cm. From the bottom to the top, there are water, skin, tumor, fat and muscle layers exist in this region. The heating source locates below $z=0$ cm on the xy plane. The white lines on the figure defines the contours of these different layers. The x axis is parallel with the waveguide, the result region is same size of the waveguide,

which is 10cm due to the penetration depth. The highest temperature appears at the center of x axis in the tumor layer. Temperature rise in fat can be as high as 6°C, which will do no harm to human body cause it is in fat layer. And the heated region in fat is very small while in tumor is bigger. The temperature rise in the skin is around 4 °C, which is in the region that patient could bare with. The color bar shows the temperature rise corresponding to the color in the result figure. The temperature rise in muscle layer is below 0.5 °C.

The bottom figure shown about the YZ plane has similar format with the result figure on xz plane. The white lines define the contour of diffrent layers of water, skin, tumor, and fat. The temperature rise focuses on the tumor layer and locates in the center of the waveguide covered region. The fat is heated partially because the orientation of the waveguide is not parallel with the surface of the human body. The contour of the white line illustrate curves in human chest, which can not be ideally parallel with the waveguide orientation. However, the highest temperature rise in fat is below 6 °C, which is acceptable for human body.

When 2cm thickness tumor layer phantom is inserted under the skin layer of the human model, add the water bolus from 3cm to 6cm in the model. Obtain different electromagnetic power depositions for these four different water bolus thicknesses. The best water bolus thickness 5cm gives the best TD90 with a specific treatment time. The temperature distribution on XZ plane and YZ plane are shown in the Fig. 4.4 for 2cm thickness of tumor layer and 5cm thickness of water bolus. The coordinates is same as the one shown in 2.5. XZ plane shows the top view of the chest while YZ plane shows the side view of the chest. The top figure shows the temperature distribution on XZ plane which locates at the center of the waveguide. Along Z axis, the region length is 8cm. From the bottom to the top, there are water, skin, tumor, fat and muscle layers exist in this region. The heating source locates below z=0cm on the xy plane. The white lines on the figure defines the

contours of these different layers. Along the x axis the result region is 10cm due to the penetration depth. In this way, the temperature distribution is clear in different layers in *XZ* plane. The highest temperature appears at the center of x axis in the tumor layer. The temperature rise focus on the tumor layer since the tumor layer thickness increase. Temperature rise in fat locates in a very small region.

The bottom figure shown about the *YZ* plane has similar format with the result figure on *xz* plane. The white lines define the contour of different layers of water, skin, tumor, and fat. The temperature rise focuses on the tumor layer and locates in the center of the waveguide covered region. The fat is heated only for a small part cause the tumor thickness increase. Even the orientation of the waveguide is not parallel with the surface of the human body, the hot spot is a small region due to the applicator penetration depth.

Both *XZ* and *YZ* plane locates at the center of the waveguide, which means these two figures shows the largest heated planes in human body. The temperature rise in the skin and fat is around 4 °C, which falls in the temperature region that patient could bare with. The color bar shows the temperature rise corresponding to the color in the result figure. The temperature rise in muscle layer is below 0.5 °C. In total, the temperature pattern in human body is suitable for hyperthermia.

When tumor phantom thickness increase to 3cm, add the water bolus of 3cm, 4cm, 5cm and 6cm into the model. Simulation results show 4cm water bolus thickness gives the best thermal dose for 3cm tumor layer when circulating water temperature is 37 °C. The temperature distribution on *XZ* plane and *YZ* plane are shown in the Fig. 4.5 for 3cm tumor layer with 4cm thickness of water bolus. The coordinates is same as the one shown in 2.5. *XZ* plane shows the top view of the chest while *YZ* plane shows the side view of the chest. The top figure shows the temperature distribution on *XZ* plane which locates at the center of the waveguide. Along *Z* axis, the region length is 8cm. From the bottom to the top, there are water, skin, tumor, fat and

muscle layers exist in this region. The heating source locates below $z=0\text{cm}$ on the xy plane. The white lines on the figure defines the contours of these different layers. Along the x axis the result region is 10cm due to the penetration depth. In this way, the temperature distribution is clear in different layers in XZ plane. The highest temperature appears at the center of x axis in the tumor layer and is 1cm below the skin surface. The region of temperature rise above 5°C locates at 2cm below the skin on this XZ plane. The color bar shows the temperature rise corresponding to the color in the result figure.

The bottom figure shown about the YZ plane has similar format with the result figure on XZ plane. The white lines define the contour of different layers of water, skin, tumor, and fat distribution on this YZ plane. The temperature rise focuses on the tumor layer and locates in the center of the waveguide covered region. On this plane, even the human contour has a curve and the orientation of the waveguide is not parallel with the surface of the human body, all the temperature rise focus on the tumor layer. The temperature rise in fat or skin layer is below 4°C , which will do no harm to human tissue.

Both XZ and YZ plane locates at the center of the waveguide, which means these two figures shows the largest heated planes in human body. From these two figures, the heated region focuses on the center of the waveguide on XY plane and 2cm below the skin layer. When the tumor size is over 3cm , the temperature rise in the skin and fat is below 4°C and only a very small part of the fat layer is heated. The temperature rise in muscle layer is below 0.5°C . In total, the temperature pattern in human body is suitable for hyperthermia.

All these three sets of temperature distribution shows the heating pattern for the waveguide. For 1cm tumor layer, 3cm water bolus gives the best thermal dose. 2cm tumor with 5cm water bolus and 3cm tumor with 4cm water bolus give the best thermal dose. If the tumor is equal or above 2cm , then the heated region over 5°C

is 2cm deep from the skin layer. And the temperature rise in 3cm is as high as 4 °C. When the tumor layer is 1cm, more unwanted heat is generated in the fat layer if there is obvious curve on the patient contour. However, the hot spot in fat is small enough to do no harm to patient. For different tumor thickness, the temperature in the center of the tumor is elevated by about 7 degrees while the temperature increase in muscle is negligible. Then for real patient model, the study focuses on the 1cm tumor phantom. If there is no severe hot spot in 1cm, the configuration would not have any hot spot when the tumor layer is thicker. Meanwhile, 1cm thickness appears more often than 2cm or 3cm. The heated region above 4 °C localizes in a 5cm by 5cm region on the axis of the waveguide with the highest temperature rise is 7 °C. To solve this problem, the temperature of the water is optimized to increase the heated region. Meanwhile, the waveguide size is increased. The water bolus thickness varies for different tumor layer thickness to give the best thermal dose, which can be easily implemented by the robotic arm system.

4.2.2 Spiral Antenna Heating Effect

This section studies the heating pattern for spiral antenna. The human tissue model is derived in the same way which is described in section 4.2.1. Instead of modeling a waveguide, an Archimedean spiral antenna is modeled here excited by the probe from the back center. The antenna operates on 433MHz. For 1cm thickness tumor phantom, the water bolus thickness is selected as 3cm. Then the distance between the spiral antenna and the water bolus is 3cm. The temperature distribution on the center XZ and YZ plane are shown in the figure 4.6. Same as section 4.2.1, the coordinate is defined in 2.5. Then the XZ plane shows the top view while YZ plane shows the side view of the chest. In Fig. 4.6, the top one shows the temperature distribution on XZ plane on the axis of the origin point of the spiral antenna. The white lines in the figure define the different layers of human tissue. Since the human

model is same as the one in waveguide model, then from the bottom to the top there are water, skin, tumor, fat and muscle layers. The diameter of the spiral is about 9.5cm, due to the penetration depth, the result figure shows 10cm along X axis and Y axis. The spiral antenna locates at the XY plane, which is parallel with the X axis at $Z=0$ cm. The temperature rise is below 2°C at 2cm below the skin. So that the result figure shows 7cm along Z axis. With the color bar which shows the corresponding color to the temperature rise, the figure shows the highest temperature rise appears in tumor. The radius of the heating region above 5°C is about 5cm along X axis. The whole tumor layer is heated above 3°C , and the temperature rise in fat and skin is all below 4°C and the heated depth is only 0.5cm in fat layer. The temperature rise in muscle layer is negligible.

The bottom figure in Fig. 4.6 shows the temperature distribution in the YZ plane with similar illustration format. The white lines define the same layer sequence as the top figure about XZ plane. The figure illustrates the heat focuses in the tumor layer. Within 6cm along Y axis the temperature rise is above 4°C .

The two figures in Fig. 4.6 show the heat pattern of XZ plane and YZ plane. All the heat focus in the tumor layer, there is no hot spot in the tumor layer even there is curve on the skin surface where the surface of the spiral antenna can not be parallel with the skin surface. And the temperature rise in the tumor region covers a larger area than waveguide.

For 2cm thickness tumor phantom, the water bolus thickness is selected as 5cm. The temperature distribution on the center XZ and YZ plane are shown in the figure 4.7. The XZ plane shows the top view while YZ plane shows the side view of the chest. In Fig. 4.7, the top one shows the temperature distribution on XZ plane on the axis of the origin point of the spiral antenna. The white lines in the figure define the different layers of human tissue. The tumor layer is thicker as 2cm, the fat layer thickness decrease which keeps the muscle distribution as before. Due to the

penetration depth, the result figure shows 10cm along X axis and Y axis, and 7cm along Z axis. The spiral antenna locates at the XY plane, which is parallel with the X axis at $Z=0$ cm. With the aid of color bar, the figure shows the highest temperature rise appears in tumor. The radius of the heating region above 4°C is about 5cm along X axis. A large part of the tumor layer is heated. The temperature rise in skin is below 4°C . The temperature rise in fat is below 3°C and the heated depth is only 0.5cm in fat layer. The temperature rise in muscle layer is negligible.

The bottom figure in Fig. 4.7 shows the temperature distribution in the YZ plane with similar illustration format. The white lines define the same layer sequence as the top figure about XZ plane. The figure illustrates the heat focuses in the tumor layer. When the tumor layer is 2cm thickness, the temperature rise above 5°C is as deep as 2cm in tumor. Within 5cm along Y axis the temperature rise is above 4°C .

The two figures in Fig. 4.7 show the heat pattern of XZ plane and YZ plane. When the tumor layer increase to 2cm, the lateral heating area along X and Y axis is smaller than 1cm tumor layer while the heating depth is increasing to 2cm. The temperature rise in fat decreases as the tumor layer thickness increase and no more hot spot.

For 3cm thickness tumor phantom, the water bolus thickness is selected as 4cm. The temperature distribution on the center XZ and YZ plane are shown in the figure 4.8. The XZ plane shows the top view while YZ plane shows the side view of the chest. In Fig. 4.8, the top one shows the temperature distribution on XZ plane on the axis of the origin point of the spiral antenna. Defined by the white lines, the tumor layer is thicker as 3cm and the fat layer thickness decrease. The result figure shows 10cm along X axis and Y axis, and 8cm along Z axis. The spiral antenna locates at the XY plane, which is parallel with the X axis where is below $Z=0$ cm. The highest temperature rise appears in tumor. The radius of the heating region above 4°C is about 3cm along X axis and 2cm along Z axis. When the depth is 3cm

in tumor, the temperature rise is 2°C . The temperature rise in skin is below 4°C . The temperature rise in fat is below 2°C and the heated depth is only 0.5cm in fat layer. The temperature rise in muscle layer is negligible.

The bottom figure in Fig. 4.7 shows the temperature distribution in the YZ plane with similar illustration format. Spiral antenna locates below $Z = 0\text{cm}$ and parallel with y axis.

The temperature rise above 5°C is as deep as 2cm in tumor. Within 5cm along Y axis the temperature rise is above 4°C . The radius of the heating region above 4°C is about 2.5cm along Y axis and 2cm along Z axis. When the depth is 3cm in tumor, the temperature rise is 2°C . The temperature rise in skin is below 5°C . The temperature rise in fat is below 2°C and the heated depth is only 0.5cm in fat layer. The temperature rise in muscle layer is negligible.

The two figures in Fig. 4.8 show the heat pattern of XZ plane and YZ plane. When the tumor layer increase to 3cm, the lateral heated area along X and Y axis is smaller than 1cm and 2cm tumor layer. The heating depth in tumor along Z axis is 2cm for temperature above 5°C . The temperature rise in fat decreases as the tumor layer thickness increase and no more hot spot.

Compared with the results shown in Fig.4.6, Fig.4.7 and Fig.4.8, the heating depth for the temperature over 5°C is about 2cm. When the tumor thickness increase, the lateral heated area along X and Y axis decreases, the heated region along Z axis is increasing with the maximum depth as 2cm. Skin layer is heated and the maximum temperature is 5°C with the temperature is normalized to 7°C . Compared with the waveguide, the skin temperature for spiral antenna is higher, which gives a hint about adjusting water bolus temperature in later simulation study. As the tumor layer thickness increases, the heated region in fat layer decrease.

Compared with waveguide simulation result, the spiral antenna generates no hot spot and much less heat in fat layer when the tumor layer is 1cm at the curved surface

on the skin. The heated region is larger for spiral antenna, which leads to larger TD for 1cm tumor. When the tumor thickness increases to 3cm, the heated region of waveguide is better for spiral antenna. Since the waveguide has better penetration depth, it should be used on the thick tumor region and the spiral antenna should be used for the thin tumor region. However, the skin temperature heated by spiral antenna is higher than waveguide, which can be solved by adjusting the water temperature in bolus.

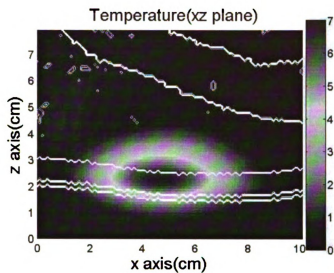
4.3 Simulation Result of Tumor on Different Location

Shown in Fig.1.1, the robotic arm is assumed to move from region 1 to 4 to cover all the chest wall region, any of which is possibly the tumor location. To achieve the best heating effect, the transverse plane of the waveguide or the surface plane of the spiral antenna should be parallel with the surface area, which is implemented by rotating the human body in the simulation. The heating pattern of waveguide on these 4 consecutive regions are also modeled in this section. Fig. 4.9, Fig. 4.10, Fig. 4.11 and Fig. 4.12 show the temperature distribution on the center XZ and YZ plane of these 4 consecutive regions. In Sec. 4.2.1, the modeled human tissue derived from region 1. All the result figures have the same format as the figures in Sec. 4.2.1.

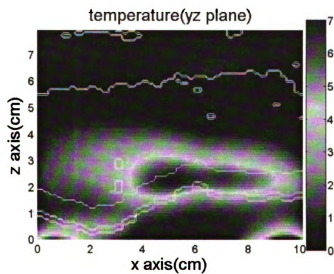
The models are derived from the human tissue of each region with 1cm tumor layer phantom and 3cm water bolus inserted in. Obtain the temperature distribution by the simulation systems built by the methods described Chap. 2. Fig. 4.9 shows the temperature distribution in the region 1, Fig. 4.10 shows region 2, Fig. 4.11 shows region 3 and Fig. 4.12 shows region 4. In each of these 4 result figures, top figure shows the temperature distribution on XZ plane located at the center of the waveguide, and the bottom one shows the YZ plane located at the center of the

waveguide. The white lines describe the contours of different layer. The waveguide locates at the XY plane below $Z = 0$. From the bottom to top, there are water, skin, tumor, fat and muscle. The temperature rise is primarily located within the tumor layer in all of these four regions. In region 2 and 3, when the applicator is on top of the chest, contact area with the applicator is larger and the thermal dose is higher. On the other hand, when the applicator is over the side of the chest, thermal dose is less due to smaller area of contact area.

According to the simulation results, the simulation system can simulate any location of the applicators, which will help the treatment plan in the future. The thermal dose is larger at the part where the body surface is flat then the one where the surface has curves. The thermal dose in the desired tumor region is larger if the waveguide or spiral antenna is parallel to the skin surface.

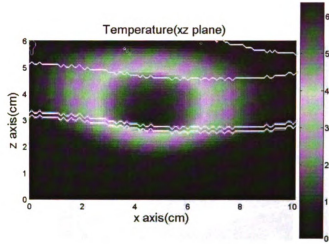


(a) xz plane

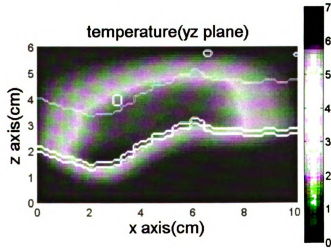


(b) yz plane

Figure 4.3. The simulated temperature distribution on the xz plane and yz plane in the center of the applicator by FDTD. The correspondent tumor layer is 1cm. The applicator applied here is a 10cm by 10cm waveguide working on 915MHz

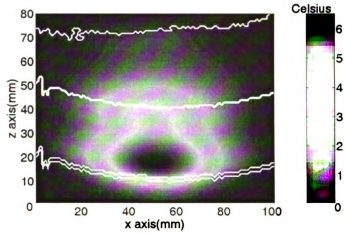


(a) xz plane

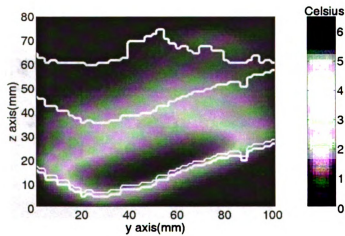


(b) yz plane

Figure 4.4. The simulated temperature distribution on the xz plane and yz plane in the center of the applicator by FDTD. The correspondent tumor layer is 2cm. The applicator applied here is a 10cm by 10cm waveguide working on 915MHz

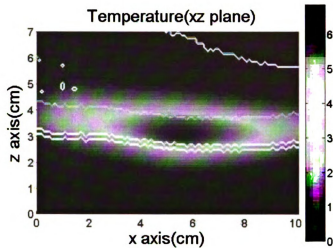


(a) xz plane

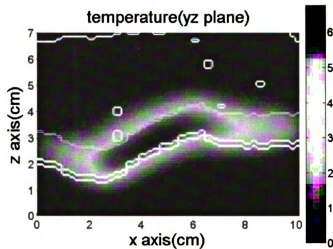


(b) yz plane

Figure 4.5. The simulated temperature distribution on the xz plane and yz plane in the center of the applicator by FDTD. The correspondent tumor layer is 3cm. The applicator applied here is a 10cm by 10cm waveguide working on 915MHz

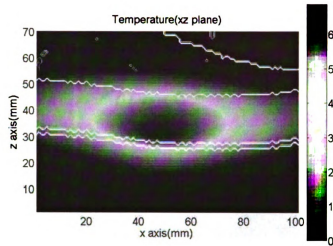


(a) xz plane

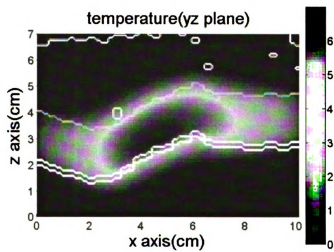


(b) yz plane

Figure 4.6. The simulated temperature distribution on the xz plane and yz plane in the center of the applicator. The tumor layer is 1cm. The applicator applied here is a 4.572cm radius spiral antenna working on 433MHz

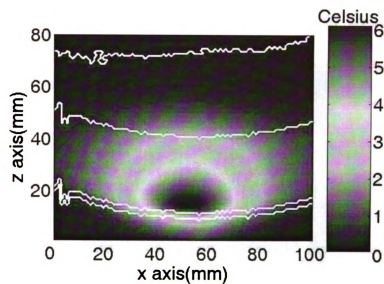


(a) xz plane

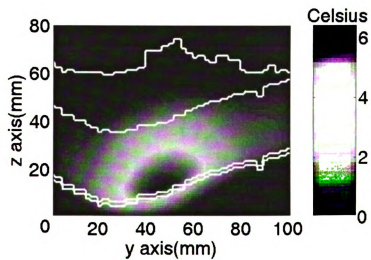


(b) yz plane

Figure 4.7. The simulated temperature distribution on the xz plane and yz plane in the center of the applicator. The tumor layer is 2cm. The applicator applied here is a 4.572cm radius spiral antenna working on 433MHz

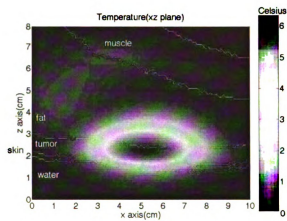


(a) xz plane

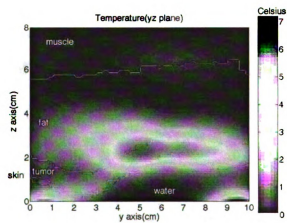


(b) yz plane

Figure 4.8. The simulated temperature distribution on the xz plane and yz plane in the center of the applicator. The tumor layer is 3cm. The applicator applied here is a 4.572cm radius spiral antenna working on 433MHz

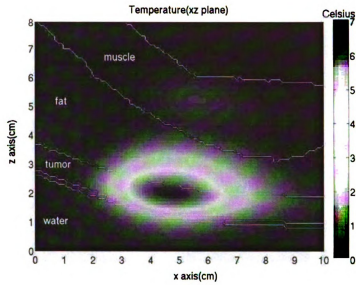


(a) xz plane

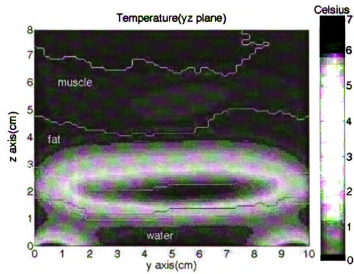


(b) yz plane

Figure 4.9. The simulated temperature distribution on the xz plane and yz plane in the center of 10cm by 10cm waveguide. The maximum temperature is 7°C. Model is derived from the REGION ONE in Fig.1.1 with 1cm tumor layer and 3cm water.

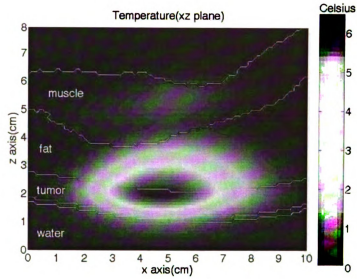


(a) xz plane

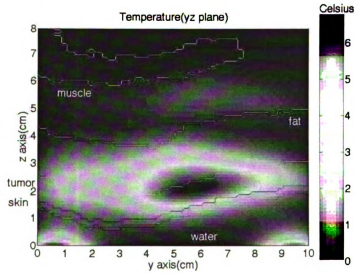


(b) yz plane

Figure 4.10. The simulated temperature distribution on the xz plane and yz plane in the center of 10cm by 10cm waveguide. The maximum temperature is 7°C. Model is derived from the REGION TWO in Fig.1.1 tissue with 1cm tumor layer and 3cm water.

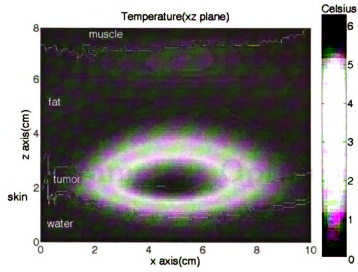


(a) xz plane

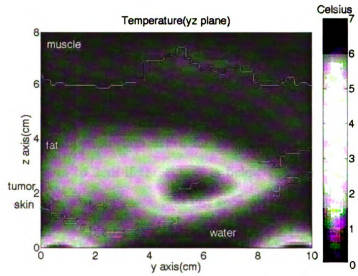


(b) yz plane

Figure 4.11. The simulated temperature distribution on the xz plane and yz plane in the center of 10cm by 10cm waveguide. The maximum temperature is 7°C. Model is derived from the REGION THREE in Fig.1.1 tissue with 1cm tumor layer.



(a) xz plane



(b) yz plane

Figure 4.12. The simulated temperature distribution on the xz plane and yz plane in the center of waveguide. The maximum temperature is 7°C. Model is derived from the REGION FOUR in Fig.1.1 tissue with 1cm tumor layer and 3cm water.

CHAPTER 5

System Parameters Optimization Results for Spiral Antenna and Waveguide

In last section, the simulation focus on studying the heating pattern of different tumor thickness and different tumor locations. In this section, the simulation focus on the optimization. When the models dervie from the health person chest images, simulation results show the penetration depth for temperature above 50C of waveguide and spiral antenna goes to 2cm if the tumor is below the skin. Since 1cm is more typical than 2cm for tumor thickness, and hot spot problem needs to be considered for 1cm tumor, then in the following simulation the tumor layer is chosen as 1cm. In this section, the models derive from the breast cancer patient whose breast has already been removed with surgery. Compared with the phantom model, the models in this chapter give more information for doctors and can be compared with the clinical results. Following simulations focus on the optimization of water bolus temperature, bolus and air gap thickness. From the simulation results shown in last section, the heated area of these two applicators are relative small. To increase the thermal dose,

the temperature of water needs to be studied. Meanwhile, the water bolus and air gap are two possible choices which are put between the applicator and the patient. The thickness effect the EM power deposition and also needs to be optimized.

5.1 Heating Effect of Spiral Antenna and Optimization

This section studies the heating pattern for spiral antenna and the optimization of the system parameters. The human tissue model is derived in the way described in section 2.5.2. An Archimedean spiral antenna operated on 433MHz is modeled here. The antenna is exactly same as the one described in Sec.4.1.

For 1cm tumor layer phantom under the skin, human tissue is modeled from the patient CT images. A set of models are generated with water bolus of 0.5cm, 1cm, 1.5cm, 2cm and 2.5cm. Compared with the thermal dose of these applicators, 3cm water bolus gives the best result for spiral antenna. The water temperature is 37 Celcius degree for all models.

For the model in which the tumor layer is 1cm and water blous is 2cm, the power deposition is obtained by FDTD simulation. Based on the E power deposition, the water temperature and power scale is optimizeed under the standard mentioned in Chap. ???. Set the power is 1 when the applicator heat the human body to 45°C with the water temperature is 37°C. When increase the water temperature for optimization, the power scale needs to be adjusted at the same time. In the optimizaiton process, test the power scale from 0.6 to 0.9 and water temperature from 40 to 42°C.

When the heating period is 60 minutes, the highest temperature in human body, the highest temperature in skin, the percent of tumor with 5 Cumulative Equivalent Minutes(CEM) 43 °C in all the tumor cells, the percent of healthy tissue with 5 CEM

<i>Power Scale</i>	<i>Highest Temp. in Human</i>	<i>Highest Temp. in Skin</i>	<i>Tumor % with 5 CEM</i>	<i>Health Tissue % with 5 CEM</i>
0.6	5.71	40.1	1.0	29.0
0.7	6.51	40.3	2.4	45.6
0.8	7.31	40.5	4.1	61.0
0.9	8.11	40.7	6.1	74.8
1.0	8.91	40.8	8.1	83.5

Table 5.1. Parameters Study for Power Scale when Water Temperature is 40°C

<i>Power Scale</i>	<i>Highest Temp. in Human</i>	<i>Highest Temp. in Skin</i>	<i>Tumor % with 5 CEM</i>	<i>Health Tissue % with 5 CEM</i>
0.6	6.1	40.8	2.2	54.7
0.7	6.8	41.0	3.9	72.4
0.8	7.6	41.1	5.8	85.0
0.9	8.4	41.4	8.0	92.2
1.0	9.2	41.5	10.0	95.6

Table 5.2. Parameters Study for Power Scale when Water Temperature is 41°C

<i>Power Scale</i>	<i>Highest Temp. in Human</i>	<i>Highest Temp. in Skin</i>	<i>Tumor % with 5 CEM</i>	<i>Health Tissue % with 5 CEM</i>
0.6	6.6	41.5	4.6	82.0
0.7	7.3	41.7	6.2	91.7
0.8	8.0	41.9	8.1	96.2
0.9	8.8	42.0	10.0	98.2
1.0	9.5	42.2	11.8	99.1

Table 5.3. Parameters Study for Power Scale when Water Temperature is 42°C

43 °C in the healthy tissue like fat muscle and skin for the varied water temperature and power scale is listed in the Table 5.1, 5.2 and 5.3.

Look through these tables and compare with the optimization standards. First rule is that the highest temperature in human body should be below 45°C. Patient skin can only bare with 43°C. And The health tissue over 5 CEM should be lower than 10 percent. Under these rules, choose the water temperature and power scale which gives the biggest thermal dose. The best temperature in the table is 42°C and power scale is 0.7. However, in the hospitals, the doctors are more conservative and they use the temperature under 42°C. Then the water temperature is chosen as 41.5 Celcius and power scale is 0.7. Degree and the optimized thermal dose is 7 minutes. The table show a trend that the water temperature in the bolus has a greater effect on the thermal dose than the power scale. This result is obvious with the simulation result in last section. The heated region is a small part in tumor, if the water temperature increase, then the tumor under the skin would be heated for the heat flux. Then in the following optimization procedure, the water bolus temperature optimization starts at 42°C, which would save the simulation time.

In the optimized configuration where the water bolus is 3cm and the water temperature is 41.5°C, the simulated temperature distribution on the center *XZ* and *YZ* plane are shown in the figure 5.1. The coordinate is defined in 2.5. *XZ* plane shows the top view while *YZ* plane shows the side view of the chest. In Fig. 5.1, the top one shows the temperature distribution on *XZ* plane where the highest temperature are. The white lines in the figure define the different layers of human tissue. From the bottom to the top there are water, skin, tumor, fat and muscle layers. The diameter of the spiral is about 9.5cm, due to the penetration depth, the result figure shows 10cm along *X* axis and *Y* axis. The spiral antenna locates at the *XY* plane, which is parallel with the *X* axis at *Z*=0cm. The penetration depth according to last section is 2cm under the skin . Then the result figure shows 7cm along *Z* axis. With the color

bar which shows the corresponding color to the temperature rise, the figure shows the highest temperature rise appears in tumor. The radius of the heating region above 42°C is about 10cm along X axis. The temperature in fat goes as high as 43.5°C the heated depth is 1.5 along X axis. The skin temperature is 41.5°C . The temperature rise in muscle layer is negligible.

The bottom figure in Fig. 4.6 shows the temperature distribution in the YZ plane where the highest temperature are with similar illustration format. The white lines define the same layer sequence as the top figure about XZ plane. The figure illustrates the temperature rise is primarily located within in the tumor layer. Within 6cm along Y axis the temperature rise is above 43°C .

The two figures in Fig. 4.6 show the heat pattern of XZ plane and YZ plane. The heat focus in the tumor layer, however there is hot spot in the fat layer, which is caused by two reason. First, the water bolus temperature rise increase the temperature depth. On the other hand, this human model is derived from patient, where some part of the body has more than 1cm thickness of tumor. Then the heat would focus on the thick tumor region, where there is no fat. From the simulation result of the health patient, the spiral antenna would bring very little hot spot. So that the hot spot here is cause by the thick tumor and increase the thermal dose.

5.2 Heating Effect of Waveguide and Opimization

This section studies the heating pattern for waveguide and the optimization of the system parameters. The human tissue model is derived in the way desribed in section 2.5.2. A 10cm by 15cm waveguide operated on 915MHz is modeled here. The human tissue is derived from the patient CT images with 1cm tumor layer phantom under the skin.

<i>Water Bolus Thickness</i>	<i>Total CEM 43 T90</i>	<i>Average T90 C</i>	<i>Highest Temperature</i>
0.5cm	0.92	41.6	44.6
1cm	0.82	41.48	44.6
1.5cm	0.79	41.4	44.6
2cm	0.80	41.39	44.7
2.5cm	0.72	41.4	44.6
3cm	0.82	41.2	44.7

Table 5.4. Parameters Study for Water Bolus Thickness when Water Temperature is 42°C

5.2.1 Water Bolus Only

To study the parameters of water bolus thickness, a set of models are generated with water bolus of 0.5cm, 1cm, 1.5cm, 2cm, 2.5cm and 3cm. The simulations give the thermal dose minute for 90 percent of tumor, the average temperature in 90 percent of tumor and the highest temperature in the human body are listed in the Table.5.4. According to the sec.??, higher water temperature leads to the bigger thermal dose. Here water temperature is chosen as the 42°C.

Look through the Table.5.4, the 0.5cm water bolus gives the best thermal dose as about 1min with the highest temperature in human body as 44.6°C. So that 0.5cm is chosen as the optimized thickness. When the water bolus is 0.5cm, the water temperature is 42°C, the simulated temperature distribution is shown in Fig.5.2. The top figure shows the temperature distribution on *XZ* plane in the center of the waveguide. The coordinate is defined in 2.5, in which the *XZ* plane shows the top view of human chest. The white lines in the figure define the different layers of human tissue. From the bottom to the top there are water, skin, tumor, fat and muscle layers. The result figure size is chosen according to the applicator's size. The waveguide is 15cm along *X* axis, then the top figure shows 22cm along *X* axis. And due to penetration depth, the result figure shows 7cm along *z* axis. The waveguide locates

<i>Air Gap Thickness</i>	<i>Total CEM 43 T90</i>	<i>Average T90 C</i>
0.5cm	0.11	40.1
1cm	0.13	40.2
1.5cm	0.14	40.3
2cm	0.15	40.4

Table 5.5. Parameters Study for Air Gap Thickness when Air Temperature is 37°C

at the XY plane below $Z=0\text{cm}$. The highest temperature appears in tumor layer. The radius of temperature above 43°C is along X axis is 10cm and the penetration depth is 2cm. Temperature rise in fat can be as high as 43°C, which will do no harm to human body cause it is in fat layer. The temperature rise in the skin is around 42 °C, which is in the region that patient could bare with. The temperature rise in muscle layer is negligible.

The bottom figure shows the temperature distribution in the YZ plane with similar illustration format. According to the coordinate defined in 2.5. YZ plane shows the side view of the chest. The white lines define the same layer sequence as the top figure about XZ plane. Similarly, the highest temperature appears in tumor layer. The radius of temperature above 43°C is along Y axis is 7cm and the penetration depth is 2cm. Temperature rise in fat can be as high as 43°C, which will do no harm to human body cause it is in fat layer. The temperature rise in the skin is around 42 °C, which is in the region that patient could bare with. The temperature rise in muscle layer is negligible.

5.2.2 Air Gap Only

When clinic apply the waveguide for the superficial tumor, the waveguide sometimes does not touch the water bolus directly, which means the air gap exist between the water bolus and applicator. To study how the air would effect the EM field distri-

bution in human body, the air is modeled as surrounding the human tissue in stead of water. The model is built same as the water bolus surrounded the human body mentioned at the beginning of this section. The human tissue is derived from patient CT images. The waveguide is 10cm by 15cm operated on 915MHz. The tumor layer phantom is under the skin with 1cm thickness. The air gap thickness is below 3cm according to clinical experience. In the parameters study here, the air gap parameters here are chosen as 0.5cm, 1cm, 1.5cm and 2cm. The air gap is chosen as 37°C. If the surrounding temperature is 37°C, then there is no heat flux between the surrounding area and the human body. Under this condition, the heating pattern is only generated by the applicator. The 37°C can be implemented as heating the evaporation around the human body.

The simulations give the thermal dose minute for 90 percent of tumor and the average temperature in 90 percent of tumor in the human body are listed in the Table.5.5. From this table, the 2cm air gap gives the best thermal dose T90 minutes. The air gap distance means the shotest distance between the human body and the surface of the waveguide.

When the air gap is 2cm, the water temperature is 37°C, the simulated temperature distribution is shown in Fig.5.3. The result figure use the similar format as before. The top figure shows the temperature distribution on XZ plane in the center of the waveguide. The coordinate is defined in 2.5, in which the XZ plane shows the top view of human chest. The white lines in the figure define the different layers of human tissue. From the bottom to the top there are air, skin, tumor, fat and muscle layers. The result figure size is chosen according to the applicator's size. Due to the penetration depth, the top figure shows 22cm along X axis and 7cm along z axis. The waveguide locates at the XY plane below $Z=0$ cm. The color bar shows the temperature rise corresponding to the color in the result figure. The highest temperature appears at the center of X axis in the tumor layer. The region over 42°C is only 8cm

along X axis and penetration depth is as deep as 3cm. Temperature rise in fat can be as high as 6°C , which will do no harm to human body cause 43°C is barable for fat layer. The temperature in the skin is only 37°C for the surrounding air temperature is only 37°C .The temperature rise in muscle layer is below 0.5°C .

The bottom figure shows the temperature distribution in the YZ plane with similar illustration format. According to the coordinate defined in 2.5. YZ plane shows the side view of the chest. The white lines define the same layer sequence as the top figure about XZ plane. Similarly, the highest temperature appears in the tumor layer. The region over 42°C is 6cm along Y axis and penetration depth is as deep as 2cm. Temperature in fat can be as high as 43°C , The temperature in the skin is only 37°C for the surrounding air temperature is only 37°C .The temperature rise in muscle layer is below 0.5°C .

5.2.3 Water Bolus and Air Gap

From the simulation result in last section, the penetration depth is deeper when there is air gap surrounding the tissue instead of water bolus. However, when water surround the human tissue, the thermal dose is larger and the power efficiency is higher. Then next step the simulation focus on the effection of water and air. A set of models with different water bolus thickness and air gap thickness are built. The applicator dose not contact the water bolus directly, there is air gap between. From the former simulaiton results, the water bolus and air gap thickness should be under 3cm. The chest surface is not flat, then the distance varies between the surface to the air gap. The water bolus thickess means the shortest distance between the human surface and the air gap. Assume the interface between the water bolus and air is flat, so that the air gap thickness is the distance between the applicator and water bolus.

Table 5.6 shows a set of models with different water bolus and air gap thickness. The thermal dose (CEM) for 90 percent of tumor tissue, the average temperature for

<i>water bolus Thickness</i>	<i>air gap Thickness</i>	<i>CEM 43T90</i>	<i>average temp</i>	<i>highest temp in human</i>	<i>Highest Temp in skin</i>
0.5cm	1.0cm	1.5min	41.6°C	44.0°C	42.6°C
1.0cm	1.0cm	1.1min	41.3°C	44.0°C	42.6°C
1.5cm	0.5cm	1.0min	41.3°C	44.0°C	42.7°C
2.0cm	1.0cm	0.9min	41.2°C	44.1°C	42.9°C
2.0cm	3.0cm	0.6min	40.9°C	44.0°C	42.7°C
3.0cm	1.0cm	0.6min	41.0°C	44.1°C	42.8°C
3.0cm	2.0cm	0.5min	40.8°C	44.0°C	42.7°C

Table 5.6. Parameters Study for Water Bolus Thickness when Water Temperature is 40.5°C

tumor, the highest temperature in the whole human tissue and the highest temperature in the skin is listed in the Table 5.6. The biggest thermal dose give the best combination of water gap and air gap thickness. The other parameters show this set of optimization give the acceptable temperature distribution for hyperthermia.

From Table 5.6, when the water bolus increase, the thermal dose decrease. When the air gap increase, the thermal dose decrease also. The water temperature has tried a lot for the optimization standard. When the water temperature choose as 42°C, the skin temperature is over 43°C, which is not acceptable, or the highest temperature in body is above 45°C. To satisfy the optimization standard mentioned in last chapter, the water temperature and the power scale is chosen after a big number of parameters. When the water temperature is 40.5°C, the optimized water bolus thickness is 0.5cm and the air gap thickness is 1cm.

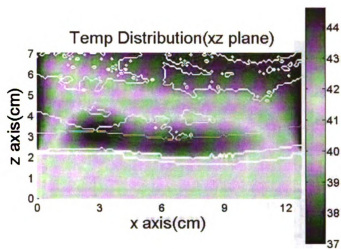
When the water gap is 0.5cm, air gap is 1cm and the water temperature is 40.5°C, the simulated temperature distribution is shown in Fig.5.4. The result figure use the similar format as other temperature distribution figures. The top figure shows the temperature distribution on *XZ* plane in the center of the waveguide. The coordinate is defined in 2.5, in which the *XZ* plane shows the top view of human chest. The

white lines in the figure define the different layers of human tissue. From the bottom to the top there are air, water, skin, tumor, fat and muscle layers. The different layer with air and water are not shown here. The result figure size is chosen according to the applicator's size. Due to the penetration depth, the top figure shows 22cm along X axis and 7cm along z axis. The waveguide locates at the XY plane below $Z=0$ cm. The color bar shows the temperature rise corresponding to the color in the result figure. The highest temperature appears at the center of X axis in the tumor layer. The region over 42°C is only 12cm along X axis and penetration depth is 2-3cm. Temperature rise in fat can be as high as 6°C , which will do no harm to human body cause 43°C is barable for fat layer. The temperature in the skin is only 37°C for the surrounding air temperature is only 37°C . The temperature rise in muscle layer is below 0.5°C .

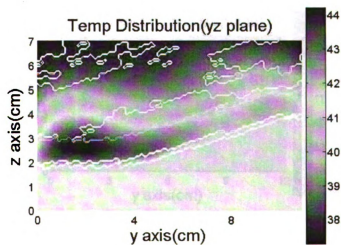
The bottom figure shows the temperature distribution in the YZ plane with similar illustration format. According to the coordinate defined in 2.5. YZ plane shows the side view of the chest. The white lines define the same layer sequence as the top figure about XZ plane. Similarly, the highest temperature appears in the tumor layer. The region over 42°C is 8cm along Y axis and penetration depth is as deep as 2cm. Temperature in fat can be as high as 43°C , The temperature in the skin is only 37°C for the surrounding air temperature is only 37°C . The temperature rise in muscle layer is below 0.5°C .

From the simulation result, when there are water and air between the human body and the waveguide, the heated region along X axis and X axis is as large as water bolus only but larger than air gap only. The combination can achieve 12cm along X axis and 8 cm along Y axis while the air gap is only 10cm by 6cm. The penetration depth is smaller than air gap only but bigger than water bolus only, which is very helpful if the tumor is very near the surface, and 3cm deep there are important tissue like muscle or organ. However, if the tumor is deep, the air gap can be considered.

Here only study the 1cm tumor, but the heating pattern can be a reference for other thickness tumor and is the future work.

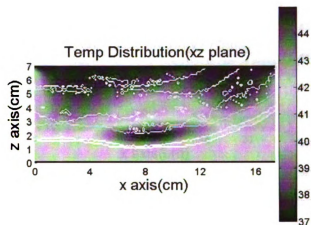


(a) xz plane

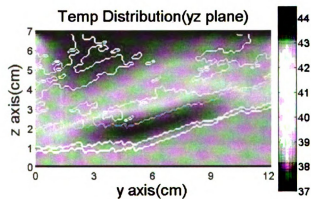


(b) yz plane

Figure 5.1. The simulated temperature distribution on the xz plane and yz plane in the center of the applicator. The model is derived from patient CT images. The applicator applied here is a 4.572cm radius spiral antenna working on 433MHz

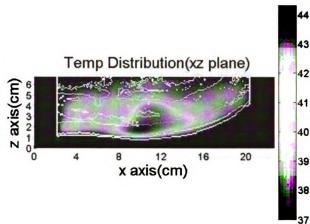


(a) xz plane

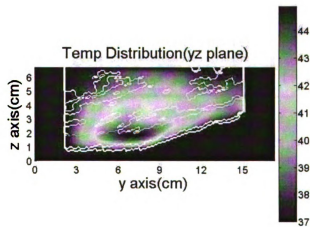


(b) yz plane

Figure 5.2. The simulated temperature distribution on the xz plane and yz plane in the center of the applicator. The model is derived from patient CT images. The applicator applied here is a 10cm by 15cm of waveguide operating on 915MHz. Only water bolus exists in the system

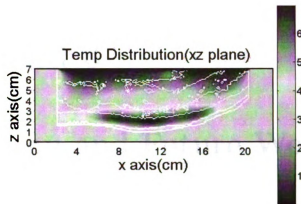


(a) xz plane

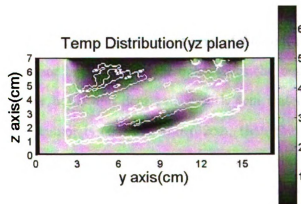


(b) yz plane

Figure 5.3. The simulated temperature distribution on the xz plane and yz plane in the center of the applicator. The model is derived from patient CT images. The applicator applied here is a 10cm by 15cm of waveguide operating on 915MHz. Only air gap exists in the system.



(a) xz plane



(b) yz plane

Figure 5.4. The simulated temperature distribution on the xz plane and yz plane in the center of the applicator. The model is derived from patient CT images. The applicator applied here is a 10cm by 15cm of waveguide operating on 915MHz. Only air gap exists in the system.

CHAPTER 6

Conclusion and Future Work

6.1 Conclusion

In this thesis, the waveguide and spiral antenna are studied for hyperthermia chest wall recurrence.

Chap.4 studied these applicators effect on tumor of different thickness and different location. For 1cm tumor layer, 3cm water bolus gives the best thermal dose. 2cm tumor with 5cm water bolus and 3cm tumor with 4cm water bolus give the best thermal dose. If the tumor is equal or above 2cm, then the heated region over 5 °C is 2cm deep from the skin layer. And the temperature rise in 3cm is as high as 4 °C. For different tumor thickness, the temperature in the center of the tumor is elevated by about 7 degrees while the temperature increase in muscle is negligible. The penetration depth above 42°C is 2cm in tumor when tumor is right under the skin layer. As the tumor layer thickness increases, the heated region along transverse surface, which means x and y direction shrinks and the heated fat region decreases. These conclusions applys to both waveguide and spiral antenna. For waveguide, the heated region above 4 °C localize in a 5cm by 5cm along the transverse surface. While for spiral antenna, the region is about 6cm by 6cm. On trasverse surface. So that

when the tumor is 1cm thickness, the heated region on trasverse surface is larger. When the tumor is thicker as 2cm or 3cm, the heated region by waveguide is larger than spiral antenna. Compared with waveguide simulation result, the spiral antenna generates no hot spot and much less heat in fat layer when the tumor layer is 1cm at the curved surface on the skin. However, The skin temperature for spiral antenna is higher. When the applicators are applied to different locations on human body, the thermal dose is larger at the part where the body surface is flat then the one where the surface has curves. The thermal dose in the desired tumor region is larger if the waveguide or spiral antenna is parallel to the skin surface.

Chap.5 focus on the optimization of the water bolus and air gap in the system. The human model is derived from CT images of chest wall recurrence patients. On the specific tumor pattern of 1cm thickness, the thickness of water bolus, air gap and their temperature is studied. Simulation results show combined water bolus and air gap bring the best thermal dose. When the water gap is 0.5cm, air gap is 1cm and the water temperature is 40.5°C, the best thermal dose is 1.5min. If water gap only, the best thermal dose TD90 is 1min, when the water bolus is 0.5cm and the water temperature is 41.5°C. And if air gap only, the best thermal dose TD is only 0.15min when the air gap thickness is 2cm with the air surrounded is only human body temperature. For 1cm tumor layer under the skin, the water and air surrounded gives the best heating effect. When there are water and air between the human body and the waveguide, the heated region along X axis and Y axis is as large as water bolus only but larger than air gap only. The combination can achieve 12cm along X axis and 8 cm along Y axis while the air gap is only 10cm by 6cm. The penetration depth is smaller than air gap only but bigger than water bolus only, which is very helpful if the tumor is very near the surface, and 3cm deep there are important tissue like muscle or organ. However, if the tumor is deep, the air gap can be considered.

6.2 Future Work

The optimization of the water bolus and air gap thickness focuses on 1cm tumor layer right under the skin. In future, the optimization should be also studied for different tumor pattern, like the 2cm, 3cm thickness tumor under the skin or the 1cm under the fat layer. These phantoms simulation result can help understanding the heating effect of different tumor patterns. With these knowledge, the doctors can make treatment plan easier.

Next step is to study the heating path of the human body whole chestwall. The chest wall recurrence usually covers the whole chest wall. Usually applicator can not heat the tumor site all at once and need the help of robot arm movement. The simulation should calculate the time-variant temperature distribution and then obtain the temperature distribution even after heating. These information can help doctors determine the applicator movement later.

BIBLIOGRAPHY

- [1] , "Breast Cancer Facts and Figures 2005-2006", American Cancer Society.
- [2] , A.Chagpar, et. al. "Chest Wall Recurrence After Mastectomy Does Not Always Portend a Dismal Outcome", *Annals of Surgical Oncology*, **10**, pp. 628-634, 2003.
- [3] , J.Carl Kumaradas and Michael D. Sherar, "Finite Element Method Aided Design of a Beam Shaping Hyperthermia Microwave Applicator", *IEEE 22nd Annual EMBS International Conference*, pp. 284-287, 2000
- [4] , J. Wiersma and J. D. P. Van Dijk,"RF hyperthermia array modelling; validation by means of measured EM field distributions",*INT. J. HYPERTHERMIA*, **17**(1), pp.63-81,2001
- [5] , Tanabe, E.; McEuen, A.H.; Caslow, S.; Norris, C.S.; Samulski, T.V.; Fessenden, P. "Microstrip Spiral Antenna for Local Hyperthermia" *IEEE Microwave Symposium Digest, MTT-S International***84**(1) pp. 133 - 134, May 1984
- [6] ,T.C.Cetas, M.K.Gopal, and E.J.Gross "Current Sheet Applicators are Effective in the Hyperthermia Clinic", *IEEE* **62**(1), pp.1464-1465, 1993
- [7] , Edward A. Gelvich and Vladimir N.Mazokhin, "Contact Flexible Microstrip Applicators (CFMA) in a Range From Microwaves Up to Short Waves ", *IEEE trans. on Bio. Eng.*, **49**(9), pp.1015-1023, 2002
- [8] ,R. H. Johnson, A. W. Preece, J. W. Hand, AND J. R. James "A New Type of Lightweight Low-Frequency Electromagnetic Hyperthermia Applicator", , *IEEE, M.T.T* **35**(12), pp.1317-1321,1987
- [9] ,E.R.Lee, T.R.Wilsey, P.T. Hornorch, D.S.Kapp, P.Fessenden, A.Lohrbach, and S.D.Prionas, "Body Conformable 915 MHz Microstrip Array Applicators for Large Surface Area Hyperthermia", *IEEE trans. on Bio. Eng.*,**39**(5), pp.470-483, 1992

- [10] ,P. R. Stauffer,F. Rossetto, M.Leoncini, and G. B. Gentili, "Radiation Patterns of Dual Concentric Conductor Microstrip Antennas for Superficial Hyperthermia", *IEEE trans. on Bio. Eng.*,**45**(5), pp.605-613, 1998
- [11] , Svein Jacobsen, A.Murberg and Paul R. Stauffer, "Characterization of a Transmitting Antenna Concept for Microwave Heating and Thermometry of Superficial Tumors", *Progress In Electromagnetics Research, PIER*, **18**,pp.105-125, 1998
- [12] , Svein Jacobsen, Paul R. Stauffer, and Daniel G. Neuman, "Dual-Mode Antenna Design for Microwave Heating and Noninvasive Thermometry of Superficial Tissue Disease", *IEEE trans. on Bio. Eng.*, **47**(11), pp.1500-1509, 2000
- [13] , A. Taflov, S. C. Hagness "Computational Electrodynamics: The Finite-Difference Time-Domain Method",*Artech House*, 2000.
- [14] H. Kroeze, J. B. Van de Kamer, A. A. C. De Leeuw and J. J. W. Lagendijk "Regional hyperthermia applicator design using FDTD modeling", *Phys. Med. Biol.*, **46**(7), pp. 1919-1935, 2001.
- [15] , H.H.Pennes, Analysis of Tissue and Arterial Blood Temperature in the Resting Human Forearm," *J. of Applied Physiology*, **1**, pp. 93-102, 1948.
- [16] J. P. Berenger, "Three-Dimensional Perfectly Matched Layer for the Absorption of Electromagnetic Waves" *J. Computational Physics*, **127**(0181), pp. 363-379, 1996
- [17] S. M. Foroughipoul and K. P. Esselle, "The theory of a Singularity-Enhanced FDTD Method of Diagonal Metal Edges", *IEEE Transactions on Antennas and Propagation*, **51**(2), pp. 312-321, 2003
- [18] W. T. Joines, Y. Zhang, C Li, and R. L. Jirtle, "The Measured Electrical Properties of Normal and Malignant Human tissues from 50 to 900 MHz", *Med. Phys.*, **21**(4), pp.547-550,1994.
- [19] Ellen L. Jones et.al "Thermochemoradiotherapy Improves Oxygenation in Locally Advanced Breast Cancer", *North Carolina Clinical Cancer Research*,**10** pp.4287-4293, July 1, 2004 2004 American Association for Cancer Research
- [20] Dewhirst MW, et.al "Links RTOG quality assurance guidelines for clinical trials using hyperthermia", *Int J Radiat Oncol Biol Phys.*, **18**(5), pp.1249-59, 1990

MICHIGAN STATE UNIVERSITY LIBRARY



3 1293 02845 678